Non-intrusive imprecise stochastic simulation by line sampling

Jingwen Song[a,c], Marcos Valdebenito[b,c], Pengfei Wei[a*, c], Michael Beer[c,d,e] and Zhenzhou Lu[a]

[a] *Northewestern Polytechnical University, West Youyi Road 127, Xi'an 710072, Shaanxi, China*

[b]*Departmento de Obras Civiles, Universidad Tecnica Federico Santa Maria, Av. Espaῆa 1680, Valparaiso, Chile*

[c]*Institute for Risk and Reliability, Leibniz University Hannover, Callinstr. 34, 30167 Hannover, Germany*

[d] *Institute for Risk and Uncertainty, University of Liverpool, Peach Street, L69 7ZF, Liverpool, United Kingdom*

[e]*International Joint Research Center for Engineering Reliability and Stochastic Mechanics, Tongji University, Shanghai 200092, China*

Abstract: The non-intrusive imprecise stochastic simulation (NISS) is a general framework for the propagation of imprecise probability models and analysis of reliability. The most appealing character of this methodology framework is that, being a pure simulation method, only one precise stochastic simulation is needed for implementing the method, and the requirement of performing optimization analysis on the response functions can be elegantly avoided. However, for rare failure events, the current NISS methods are still computationally expensive. In this paper, the classical line sampling developed for precise stochastic simulation is injected into the NISS framework, and two different imprecise line sampling (ILS) methods are developed based on two different interpretations of the classical line sampling procedure. The first strategy is devised based on the set of hyperplanes introduced by the line sampling analysis, while the second strategy is developed based on an integral along each individual line. The truncation errors of both methods are measured by sensitivity indices, and the variances of all estimators are derived for indicating the statistical errors. A test example and three engineering problems of different types are introduced for comparing and demonstrating the effectiveness of the two ILS methods.

Keywords: Uncertainty quantification; Imprecise probability models; Line sampling; Sensitivity analysis; Aleatory uncertainty; Epistemic Uncertainty

1. Introduction

Uncertainty quantification (UQ) is the process of quantitatively characterizing the uncertainty of any non-deterministic quantities of interest in numerical simulation. Generally, two kinds of UQ tasks are concerned. The first task is forward UQ (also called uncertainty propagation), which aims at propagating the uncertainty characterization models from model inputs to outputs, so as to properly characterizing the uncertainties of model outputs, and further to perform risk and reliability analysis. The second task is backward UQ (also called model updating), which focuses on inferring and updating the uncertainty characterization models of model inputs based on experimental measurements of responses [1]. To implement the above UQ tasks, three groups of uncertainty characterization models have been developed, i.e., the precise probability model, the non-probabilistic models and the imprecise probability models.

Forward UQ based on precise probability models has been widely studied, and a plenty of numerical methods, such as the analytical methods based on Taylor series [2], the spectral representations [3], the stochastic simulation methods [4], and the probability density evolution method [5], have been developed, and shown to be effective for both response uncertainty characterization and

* Corresponding author: pengfeiwei@nwpu.edu.cn

reliability analysis. However, for generating precise probability models, plenty of accurate data is commonly required, which is almost impossible in real-world applications. To deal with this challenge, several kinds of non-probabilistic models, such as the interval/convex models and the fuzzy set theory, have been proposed, and numerical methods, such as the intrusive interval finite element analysis as well as the non-intrusive optimization methods [6]. The non-probabilistic models are simple but can be especially useful when the available data is extremely scarce and/or imprecise. The criticisms of non-probabilistic models are commonly twofold. Firstly, in terms of forward UQ, the intrusive methods are commonly problem-dependent and can be of limited application, while the non-intrusive optimization-based methods may be computationally expensive and perhaps impractical, especially when the limit state functions (LSF) are not convex [6]. Secondly, due to scarcity, incompleteness, imprecision of available data, two kinds of uncertainties, termed as aleatory uncertainty and epistemic uncertainty, are commonly present for each model parameter, and plenty of studies have shown that it is necessary to distinguish between these two kinds of uncertainties [7], however, non-probabilistic models commonly fail to realize this.

To fill the above-mentioned gap, the imprecise probability models such as the probability-box (p-box) model, evidence theory, and fuzzy probability model, have been devised [8], and shown to be able to separately and correctly characterize the two kinds of uncertainties in a unified model framework, thus attracting substantial attention. The numerical methods which have been developed for propagating imprecise probability models can also be divided into two groups depending on whether they are intrusive or non-intrusive. The most well-known intrusive method is the interval Monte Carlo simulation (MCS) [9], which is based on firstly generating interval samples, and then estimating the bounds of model responses for each interval sample based on, e.g., interval finite element analysis. The non-intrusive optimization-based methods have also been developed. For example, in Ref. [10], the subset simulation combined with optimization has been extended for estimating the failure probability bound; in Ref. [11], the first-order and second-order reliability methods combined with an optimization procedure have been extended to reliability analysis associated with evidence theory. All these methods need to perform double-loop optimization solver on model response function, thus compared with the propagation of precise probability models, they are computationally much more expensive, and sometimes the global convergence cannot be achieved especially when the LSFs are non-convex and/or non-differentiable.

The non-intrusive imprecise stochastic simulation (NISS) is a non-intrusive methodology framework for efficiently propagating the imprecise probability models [12][13], which has been recently developed based on the extended Monte Carlo simulation [14] and high-dimensional model representation (HDMR) [15][16]. Two groups of NISS methods, i.e., the local NISS and the global NISS, have been developed, and the subset simulation has been injected into both methods so as to perform reliability analysis subjected to rare failure events [13]. The NISS owns several advantages. Firstly, the computational cost is the same as the one involved in precise stochastic simulation, thus is much lower than the above-mentioned methods. Secondly, two kinds of potential estimation errors are properly assessed. Thirdly, there is no need to perform optimization on LSF. Thus, the NISS is an appealing method for forward UQ of imprecise probability models.

The aim of this work is to inject the line sampling [18][19], originally proposed as a generalization of axis-parallel importance sampling method for reliability analysis in precise probability models [20][21], to the local NISS framework, so as to efficiently estimate the failure probability functions associated with rare failure events. Based on the different interpretations of the classical line sampling, we developed two imprecise line sampling (ILS) procedures to achieve this target. The first strategy is motivated by the rationale that the line sampling can be regarded as repeated first-order reliability analysis, and the developed method is termed as hyperplane-based ILS. The second strategy is based on the interpretation that a line sampling analysis can be regarded as the combination of a Monte Carlo simulation in an (*n*-1)-dimensional space and a one-dimensional integral along each line, and the corresponding proposed method is called Weighted-integral ILS. The two developed ILS methods are presented in detail and compared with both analytical and real-world engineering examples. Results show that both methods are highly efficient when the LSF is weakly or mildly non-linear.

The rest of this paper is organized as follows. Section 2 briefly reviews the backgrounds of imprecise stochastic simulation and line sampling, followed by the developments of the two ILS methods in section 3. A numerical test example and three real-world civil engineering examples are introduced in section 4 for demonstrating and comparing the proposed methods. Section 5 gives conclusions.

2. Background of imprecise stochastic simulation and line sampling

2.1 Problem statement

The performance function of the structure of interest is denoted by $G = g(\boldsymbol{x})$ with $\boldsymbol{x} = (x_1, \cdots, x_n)$ being the n-dimensional input variables. For reliability analysis, the failure domain is defined as $F = \{\boldsymbol{x} : g(\boldsymbol{x}) < 0\}$, and the failure indicator function $I_F(\boldsymbol{x})$ is defined by $I_F(\boldsymbol{x})$=1 if $\boldsymbol{x} \in F$; else, $I_F(\boldsymbol{x})$=0. Let $f_{\boldsymbol{X}}(\boldsymbol{x} \mid \boldsymbol{\theta})$ denote the joint probability density function (PDF) of $\boldsymbol{x}$, and $\boldsymbol{\theta} = (\theta_1, \cdots, \theta_i, \cdots, \theta_m)$ refers to the vector of distribution parameters.

In classical reliability analysis, $\boldsymbol{\theta}$ is precisely determined as constant values, and the failure probability P_f can be formulated by the *n*-dimensional integral $P_f = \int I_F(\boldsymbol{x}) f_{\boldsymbol{X}}(\boldsymbol{x}) \mathrm{d}\boldsymbol{x}$. For imprecise probability models, the distribution parameters are uncertain, and their uncertainty representing the epistemic uncertainty (lack of knowledge) on $\boldsymbol{x}$ can be characterized, for example, by intervals. In this situation, the failure probability will be a function of $\boldsymbol{\theta}$, which is called failure probability function with the following expression

$$P_f(\boldsymbol{\theta}) = \int I_F(\boldsymbol{x}) f_{\boldsymbol{X}}(\boldsymbol{x} \mid \boldsymbol{\theta}) \mathrm{d}\boldsymbol{x} \tag{1}$$

For simplification, suppose the input variables $\boldsymbol{x}$ are characterized by parameterized probability box (p-box), then $\boldsymbol{\theta}$ will be characterized by interval variables (usually obtained with interval estimation method). Note that the above assumption doesn't imply that the proposed methods are restricted to p-box. In fact, they are applicable for any parameterized imprecise probability models. In this paper, all the input variables are assumed to be independent, and the joint PDF is expressed as $f_{\boldsymbol{X}}(\boldsymbol{x} \mid \boldsymbol{\theta}) = \prod_{d=1}^{n} f_{X_d}(x_d \mid \boldsymbol{\theta}_d)$, where $\boldsymbol{\theta}_d$ refers to the vector of the distribution parameters of x_d.

Note that the independence assumption is not crucial for the implementation of our proposed methods. they are also applicable cases with dependent inputs, which will be discussed later.

2.2 Imprecise stochastic simulation

The NISS developed in Refs. [12][13] is a non-intrusive simulation methodology framework for propagating any parameterized imprecise probability model. This framework consists of two groups of methods, where the first group of methods is termed as local NISS, and are developed based on the cut-HDMR decomposition and extended MCS procedure, while the second group of methods are global methods, and are developed based on random sampling (RS)-HDMR and a global version of extended MCS procedure. This paper is restricted to local methods.

Motivated by importance sampling, the extended MCS is based on formulating the failure probability function as [14]:

$$P_f(\boldsymbol{\theta}) = \int I_F(\boldsymbol{x}) \frac{f(\boldsymbol{x}\,|\,\boldsymbol{\theta})}{f(\boldsymbol{x}\,|\,\boldsymbol{\theta}^*)} f(\boldsymbol{x}\,|\,\boldsymbol{\theta}^*)\mathrm{d}\boldsymbol{x} \tag{2}$$

where $f(\boldsymbol{x}\,|\,\boldsymbol{\theta}^*)$ is the sampling PDF with the distribution parameters being fixed in a pre-specified point $\boldsymbol{\theta}^*$. One can refer to Ref. [14] and [22] for the specification of $\boldsymbol{\theta}^*$. Based on Eq.(2), the failure probability function can be estimated with only one set of *g*-function calls.

For improving the performance of Eq.(2) in high dimensional space and reducing the estimation errors, the HDMR is utilized to decompose the failure probability function as the sum of a series of component functions. The general HDMR formula of $P_f(\boldsymbol{\theta})$ is as follows:

$$P_f(\boldsymbol{\theta}) = P_{f0} + \sum_{i=1}^{m} P_{fi}(\theta_i) + \sum_{i=1}^{m}\sum_{j=i+1}^{m} P_{fij}(\theta_i,\theta_j) + \cdots + P_{f1,\cdots,m}(\boldsymbol{\theta}) \tag{3}$$

By using cut-HDMR method [15] to expand $P_f(\boldsymbol{\theta})$ at the fixed point $\boldsymbol{\theta}^*$, the component probability functions on the right side of Eq.(3) can be specified as

$$\begin{aligned} P_{f0} &= P_f(\boldsymbol{\theta}^*) \\ P_{fi}(\theta_i) &= P_f(\theta_i, \boldsymbol{\theta}^*_{-i}) - P_{f0} \\ P_{fij}(\theta_i,\theta_j) &= P_f(\theta_i,\theta_j,\boldsymbol{\theta}^*_{-i,j}) - P_{fi}(\theta_i) - P_{fj}(\theta_j) - P_{f0} \\ &\cdots \end{aligned} \tag{4}$$

where $\boldsymbol{\theta}^*$ is the aforementioned fixed point chosen within the support domain $\boldsymbol{\Theta}$, $\boldsymbol{\theta}^*_{-i}$ denotes the $m-1$ dimensional vector containing all elements in $\boldsymbol{\theta}^*$ except θ_i^*, and $\boldsymbol{\theta}^*_{-i,j}$ refers to the $m-2$ dimensional vector containing all elements in $\boldsymbol{\theta}^*$ except θ_i^* and θ_j^*. Based on our study, in many applications, the higher-order effects of distribution parameters are commonly not as important as the first few order effects [17][23], and representing $P_f(\boldsymbol{\theta})$ up to second-order can usually provide a satisfactory estimation, i.e.:

$$P_f(\boldsymbol{\theta}) \approx P_{f0} + \sum_{i=1}^{m} P_{fi}(\theta_i) + \sum_{i=1}^{m}\sum_{j=i+1}^{m} P_{fij}(\theta_i,\theta_j) \tag{5}$$

It is obvious that the components above can be directly estimated with classical MCS method which is actually a double-loop procedure with a heavy computational burden. NISS method [12] enables to estimate the component functions in Eq.(5) with only one set of g-function evaluations, such estimation procedure is briefly described below.

Generate N sample points $\boldsymbol{x}^{(s)}=\left(x_1^{(s)},\cdots,x_n^{(s)}\right)(s=1,\cdots,N)$ from $f_{\boldsymbol{X}}\left(\boldsymbol{x}\,|\,\boldsymbol{\theta}^*\right)$ and evaluate the corresponding values of $I_F\left(\boldsymbol{x}^{(s)}\right)(s=1,...,N)$. Then, the unbiased estimators for the first-order and second-order component functions are as follows:

$$\begin{aligned}\hat{P}_{f0}&=\frac{1}{N}\sum_{s=1}^{N}I_F\left(\boldsymbol{x}^{(s)}\right)\\ \hat{P}_{fi}\left(\theta_i\right)&=\frac{1}{N}\sum_{s=1}^{N}I_F\left(\boldsymbol{x}^{(s)}\right)r_i\left(\boldsymbol{x}^{(s)}\,|\,\theta_i,\boldsymbol{\theta}^*\right)\\ \hat{P}_{fij}\left(\theta_i,\theta_j\right)&=\frac{1}{N}\sum_{s=1}^{N}I_F\left(\boldsymbol{x}^{(s)}\right)r_{ij}\left(\boldsymbol{x}^{(s)}\,|\,\theta_i,\theta_j,\boldsymbol{\theta}^*\right)\end{aligned}\tag{6}$$

where $r_i\left(\boldsymbol{x}^{(s)}\,|\,\theta_i,\boldsymbol{\theta}^*\right)$ and $r_{ij}\left(\boldsymbol{x}^{(s)}\,|\,\theta_i,\theta_j,\boldsymbol{\theta}^*\right)$ are weight coefficients of density, and are defined as

$$\begin{aligned}r_i\left(\boldsymbol{x}^{(s)}\,|\,\theta_i,\boldsymbol{\theta}^*\right)&=\frac{f_{\boldsymbol{X}}\left(\boldsymbol{x}^{(s)}\,|\,\theta_i,\boldsymbol{\theta}^*_{-i}\right)}{f_{\boldsymbol{X}}\left(\boldsymbol{x}^{(s)}|\boldsymbol{\theta}^*\right)}-1\\ r_{ij}\left(\boldsymbol{x}^{(s)}\,|\,\theta_i,\theta_j,\boldsymbol{\theta}^*\right)&=\frac{f_{\boldsymbol{X}}\left(\boldsymbol{x}^{(s)}\,|\,\theta_i,\theta_j,\boldsymbol{\theta}^*_{-ij}\right)}{f_{\boldsymbol{X}}\left(\boldsymbol{x}^{(s)}|\boldsymbol{\theta}^*\right)}-\frac{f_{\boldsymbol{X}}\left(\boldsymbol{x}^{(s)}\,|\,\theta_i,\boldsymbol{\theta}^*_{-i}\right)}{f_{\boldsymbol{X}}\left(\boldsymbol{x}^{(s)}|\boldsymbol{\theta}^*\right)}-\frac{f_{\boldsymbol{X}}\left(\boldsymbol{x}^{(s)}\,|\,\theta_j,\boldsymbol{\theta}^*_{-j}\right)}{f_{\boldsymbol{X}}\left(\boldsymbol{x}^{(s)}|\boldsymbol{\theta}^*\right)}-1\end{aligned}\tag{7}$$

Based on Eq.(3), the estimator $\hat{P}_f\left(\boldsymbol{\theta}\right)$ is the sum of all the components in Eq.(6). In fact, higher-order component functions can also be estimated with the same set g-function evaluations if needed.

The above procedure introduces two types of errors, truncation error due to cut-HDMR truncation (e.g., Eq.(5)) and statistical error due to MCS. The statistical error, which is also a function of $\boldsymbol{\theta}$, can be estimated by computing the variances of estimators in Eq.(6) using the following expressions

$$\begin{aligned}Var\left(\hat{P}_{f0}\right)&\hat{=}\frac{1}{N\left(N-1\right)}\sum_{s=1}^{N}\left(I_F^{(s)}-\hat{P}_{f0}\right)^2\\ Var\left(\hat{P}_{fi}\right)&\hat{=}\frac{1}{N\left(N-1\right)}\sum_{s=1}^{N}\left(I_F^{(s)}r_i-\hat{P}_{fi}\right)^2\\ Var\left(\hat{P}_{fij}\right)&\hat{=}\frac{1}{N\left(N-1\right)}\sum_{s=1}^{N}\left(I_F^{(s)}r_{ij}-\hat{P}_{fij}\right)^2\end{aligned}\tag{8}$$

One the other hand, HDMR can be used to measure the relative importance of component functions, also called sensitivity analysis [24]. Ref. [17] shows the definition of sensitivity index $S_{i_1i_2\cdots i_k}$ of component functions for measuring the effect of uncertainties in distribution parameters on failure probability,

$$S_{i_1i_2\cdots i_k}=\frac{\int_{\boldsymbol{\Theta}_{i_1i_2\cdots i_k}}{P_{fi_1\cdots i_k}}^2\left(\boldsymbol{\theta}_{i_1\cdots i_k}\right)f_{\boldsymbol{\Theta}_{i_1i_2\cdots i_k}}\left(\boldsymbol{\theta}_{i_1\cdots i_k}\right)\mathrm{d}\boldsymbol{\theta}_{i_1\cdots i_k}}{\sum_{i_1\cdots i_k\in\{1,\cdots,m\}}\int_{\boldsymbol{\Theta}_{i_1i_2\cdots i_k}}{P_{fi_1\cdots i_k}}^2\left(\boldsymbol{\theta}_{i_1\cdots i_k}\right)f_{\boldsymbol{\Theta}_{i_1i_2\cdots i_k}}\left(\boldsymbol{\theta}_{i_1\cdots i_k}\right)\mathrm{d}\boldsymbol{\theta}_{i_1\cdots i_k}}\ \left|\left\{i_1i_2\cdots i_k\right\}\right|\le M\tag{9}$$

where M refers to the highest order under consideration, $f_{\boldsymbol{\Theta}_{i_1i_2\cdots i_k}}\left(\boldsymbol{\theta}_{i_1\cdots i_k}\right)$ denotes the instrumental joint PDF for $\boldsymbol{\theta}_{i_1\cdots i_k}$, for p-box case, $f_{\boldsymbol{\Theta}_{i_1i_2\cdots i_k}}\left(\boldsymbol{\theta}_{i_1\cdots i_k}\right)$ is uniform type of PDF defined with the upper and lower bound of $\boldsymbol{\theta}_{i_1\cdots i_k}$. In our previous developments, both local and global NISS methods have been developed, and in the global NISS, the Sobol' indices are used, while in the local NISS, the

sensitivity indices as shown in this paper were used since it is derived based on cut-HDMR decomposition. While cut-HDMR decomposition is utilized, the sensitivity indices utilized in this paper in fact measure the average L^2 distance of component functions to the expansion points, and the larger this distance is, the more important is this component. If the sensitivity index equals zero, then it implies that the corresponding component function always takes zero value, thus of course has no effect on the failure probability function, thus it can be eliminated in searching for the extreme values of failure probability.

Although the above procedure enables to estimate failure probability function with only one set of samples, it is still computationally intensive, especially when estimating probabilities associated with rare failure events. In Ref. [13], the subset simulation has been extended for solving this problem. However, for problems involving moderately nonlinear performance functions, line sampling can be more efficient than subset simulation from a numerical viewpoint. This motivates us to inject the line sampling into the NISS framework so that the computational cost for mildly nonlinear problems can be further reduced.

2.3 Line sampling

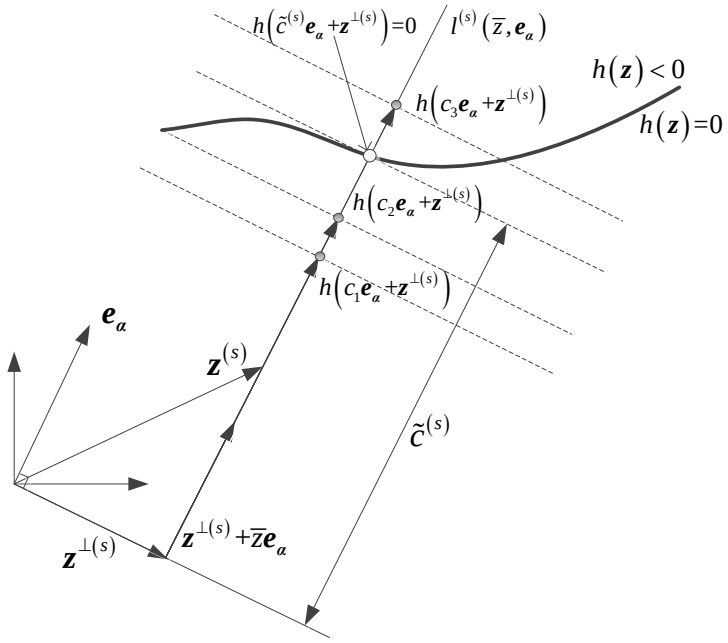

Fig.1 Rationale of Line sampling procedure in standard normal space

In precise probability framework of structural reliability analysis (epistemic uncertainty is not yet involved), line sampling is an efficient simulation method especially developed for solving a wide range applications with high-dimensional inputs and rare failure events [25]. It formulates a reliability problem as a number of conditional one-dimensional reliability problems which are analyzed in standard normal space [18]. In line sampling procedure, the important direction, which is usually defined as the negative of the steepest descent direction of LSF, must be firstly approximated. This assumption arouses one limitation that line sampling is not suitable for strong nonlinear performance functions, especially when the important direction cannot be easily estimated [26].

As mentioned above, the original space of random variables $\boldsymbol{x}$ must be transformed to standard

normal space where the new variables are denoted by $\boldsymbol{z}=(z_1,\cdots,z_n)$, similarly, the LSF $g(\boldsymbol{x})$ is then transformed to $h(\boldsymbol{z})$. The probability integral transformation (PIT) formula from original random space to standard normal space is expressed as

$$\boldsymbol{z}=\Phi^{-1}\left(F_X(\boldsymbol{x})\right) \tag{10}$$

where $F_X(\boldsymbol{x})$ is the cumulative density function (CDF) of $\boldsymbol{x}$, $\Phi^{-1}(\bullet)$ is the inverse CDF of standard normal distribution. For simplification, denote the transformation as $\boldsymbol{z}=T(\boldsymbol{x})$ and the inverse transformation as $\boldsymbol{x}=T^{-1}(\boldsymbol{z})$.

Let $\boldsymbol{\alpha}$ denote the optimal important direction, and the normalized important direction $\boldsymbol{e}_\alpha$ (which is a unit vector) is defined as follows

$$\boldsymbol{e}_\alpha=\boldsymbol{\alpha}/\|\boldsymbol{\alpha}\| \tag{11}$$

Once $\boldsymbol{e}_\alpha$ is determined, the standard normal space is orthogonally decomposed to a 1-dimensional and $n-1$ dimensional space [27], and vector $\boldsymbol{z}$ can be written as

$$\boldsymbol{z}=\boldsymbol{z}^{//}+\boldsymbol{z}^{\perp} \tag{12}$$

where $\boldsymbol{z}^{//}$ is parallel to $\boldsymbol{e}_\alpha$, and $\boldsymbol{z}^{\perp}$ is orthogonal to $\boldsymbol{e}_\alpha$, expressed as

$$\begin{aligned}\boldsymbol{z}^{//}&=\bar{z}\boldsymbol{e}_\alpha\\ \boldsymbol{z}^{\perp}&=\boldsymbol{z}-\langle\boldsymbol{e}_\alpha,\boldsymbol{z}\rangle\boldsymbol{e}_\alpha\end{aligned} \tag{13}$$

where $\langle\bullet,\bullet\rangle$ is the symbol of inner product. Since the standard Gaussian PDF is isotropic [27], the scalar $\bar{z}$ and vector $\boldsymbol{z}^{\perp}$ are also standard normally distributed.

The direct MCS is carried out by generating N_z samples $\boldsymbol{z}^{(s)}=\left(z^{(1)},\cdots,z^{(n)}\right)(s=1,\cdots,N_z)$ from its joint PDF $\phi_Z(\boldsymbol{z})$, then the $n-1$ dimensional sample vector $\boldsymbol{z}^{\perp(s)}$ can be derived with the formula $\boldsymbol{z}^{\perp(s)}=\boldsymbol{z}^{(s)}-\left\langle\boldsymbol{e}_\alpha,\boldsymbol{z}^{(s)}\right\rangle\boldsymbol{e}_\alpha$. Fig.1 provides the rationale of line sampling procedure for the s th sample in 2-dimensional standard normal space. As shown in Fig.1, the conditional failure probabilities are determined where $\boldsymbol{z}=\bar{z}\boldsymbol{e}_\alpha+\boldsymbol{z}^{\perp(s)}$ varies randomly along the line $l^{(s)}\left(\bar{z},\boldsymbol{e}_\alpha\right)$. The failure probability corresponding to $\boldsymbol{z}^{(s)}$ can be computed by

$$P_f^{(s)}=\Phi\left(-\tilde{c}^{(s)}\right) \tag{14}$$

where $\tilde{c}^{(s)}$ is the reliability index which is actually the value of $\bar{z}$ at intersection point between the LSF $h(\boldsymbol{z})=0$ and the line $l^{(s)}\left(\bar{z},\boldsymbol{e}_\alpha\right)$. Different methods can be used for this one-dimensional reliability analysis task [28]. One popular way is to consider three specific values c_1, c_2, c_3 of $\bar{z}$ so as that three points $\left(c_1,h\left(c_1\boldsymbol{e}_\alpha+\boldsymbol{z}^{\perp(s)}\right)\right)$, $\left(c_2,h\left(c_2\boldsymbol{e}_\alpha+\boldsymbol{z}^{\perp(s)}\right)\right)$ and $\left(c_3,h\left(c_3\boldsymbol{e}_\alpha+\boldsymbol{z}^{\perp(s)}\right)\right)$ are evaluated. Then $\tilde{c}^{(s)}$ can be easily determined by fitting them with second-order polynomial and determine the point $\left(\tilde{c}^{(s)},h\left(\tilde{c}^{(s)}\boldsymbol{e}_\alpha+\boldsymbol{z}^{\perp(s)}\right)=0\right)$ [29]. According to the theory of advanced first order second moment method (AFOSM) [26], in standard normal space, the reliability index $\tilde{c}^{(s)}$ is in fact the minimum

distance between the origin point and the failure boundary approximated by a hyperplane.

By collecting all the values of $\tilde{c}^{(s)}$, the MCS estimator of failure probability is

$$\hat{P}_f = \frac{1}{N_z}\sum_{s=1}^{N_z} P_f^{(s)} = \frac{1}{N_z}\sum_{s=1}^{N_z} \Phi\left(-\tilde{c}^{(s)}\right) \tag{15}$$

And the variance of the above estimator is

$$V\left(\hat{P}_f\right) = \frac{1}{N_z\left(N_z-1\right)}\sum_{s=1}^{N_z}\left(P_f^{(s)}-\hat{P}_f\right)^2 = \frac{1}{N_z\left(N_z-1\right)}\left(\sum_{s=1}^{N_z} P_f^{(s)2} - N\hat{P}_f^2\right) \tag{16}$$

Note that LSF is evaluated only when searching the value of $\tilde{c}^{(s)}$ along each line. To sum up, line sampling is an efficient simulation method based on a series of conditional one-dimensional reliability analysis, and each one-dimensional reliability analysis is implemented on MC samples from $n-1$ dimensional standard normal space orthogonal to $\boldsymbol{e}_\alpha$. From the geometric point of view, line sampling can also be regarded as carrying out N times of AFOSM reliability analysis and taking the mean of all the AFOSM results. Although the estimator of failure probability is unbiased independent from the choice of important direction, its quality (measured in terms of its variance) strongly depends on the selection of an appropriate important direction. Since the determination of important direction is not the focus of this paper, it is assumed to be known in the following part.

Further advances has been made in recent years for improving the efficiency of line sampling, such as advanced line sampling [30] to adaptively searching the important direction, and the use of surrogate model [31] to approximate the original LSF.

3. Imprecise line sampling method

In this section, we develop two different strategies for injecting the line sampling into the NISS framework for estimating the failure probability function. The first strategy is devised based on the geometric interpretation of the reliability index $\tilde{c}^{(s)}$, and is denoted as hyperplane- approximation based imprecise line sampling (HA-ILS), while the second one is developed based on the mathematical interpretation of the probability computed by integration along each line, and is called weighted-integral based imprecise line sampling (WI-ILS).

3.1 Hyperplane-approximation based imprecise line sampling

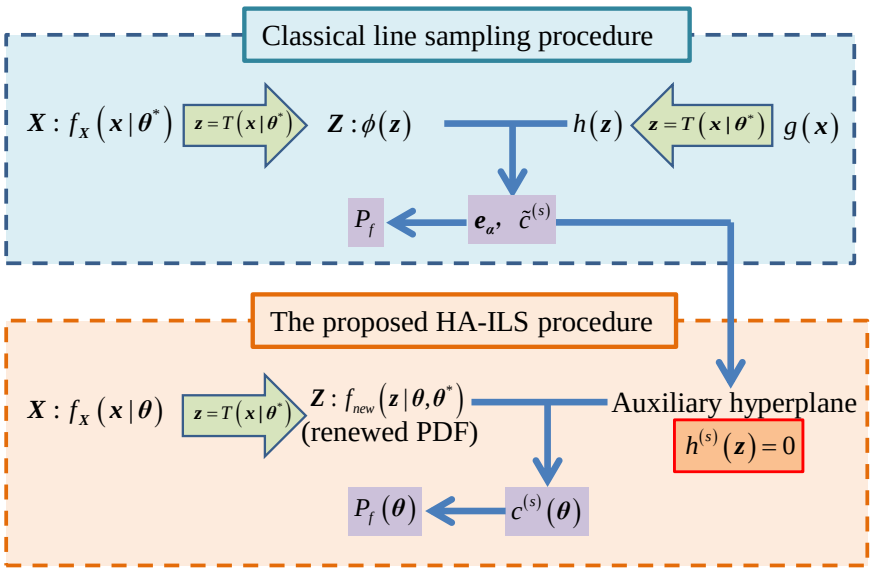

Fig.2 Sketch of the concept of hyperplane-approximation method

As mentioned in subsection 2.1, $\boldsymbol{\theta}^*$ is a fixed point chosen from the support domain of $\boldsymbol{\theta}$. In this strategy, the important direction is determined by fixing $\boldsymbol{\theta}$ at $\boldsymbol{\theta}^*$, and will be kept unchanged during the whole analysis process. This utilizes the merit of line sampling that it is unbiased, independent of the choice of important direction. As for choosing $\boldsymbol{\theta}^*$, we propose to use the same concept in Ref.[14], i.e., the support domain of $\boldsymbol{x}$ determined by the optimal $\boldsymbol{\theta}^*$ should be the same with $\boldsymbol{x}$ at the whole range of $\boldsymbol{\theta}$. In fact, $\boldsymbol{\theta}^*$ can also be specified at the point around any value of interest, as it is expected that the proposed method always performs well close to $\boldsymbol{\theta}^*$.

Fig.2 shows the general concept of the proposed HA-ILS method. First of all, classical line sampling method is applied with $\boldsymbol{\theta}$ being fixed at $\boldsymbol{\theta}^*$, shown as the upper blue box. Note that, $h(\boldsymbol{z})$ is the LSF transformed by $\boldsymbol{z}=T(\boldsymbol{x}\mid\boldsymbol{\theta}^*)$ from the original physical model, which keeps unchanged as long as the formula $\boldsymbol{z}=T(\boldsymbol{x}\mid\boldsymbol{\theta}^*)$ is fixed. There are two key concepts of the proposed method, as shown in the lower red box in Fig.2. One is to introduce auxiliary hyperplane $h^{(s)}(\boldsymbol{z})=0$ to approximate the LSF, which can be established based on the reliability index $\tilde{c}^{(s)}$ and the important direction $\boldsymbol{e}_\alpha$ (a detailed procedure for establishing $h^{(s)}(\boldsymbol{z})$ will be discussed later). The other is to renew (update) the probability distribution of $\boldsymbol{z}$ when the distribution parameters of $\boldsymbol{x}$ changes from $\boldsymbol{\theta}^*$ to $\boldsymbol{\theta}$ but the input variables $\boldsymbol{x}$ remains being transformed by the same formula $\boldsymbol{z}=T(\boldsymbol{x}\mid\boldsymbol{\theta}^*)$. For example, when x follows a normal distribution such that $N(2,2^2)$, $z=(x-2)/2$ follows standard normal distribution. Then, if the distribution of x changes to $N(4,4^2)$, $z=(x-2)/2$ no longer follows standard normal distribution, but a new distribution such that $z\sim N(1,2^2)$. As a consequence of the renewal (update) of the probability distribution, $\boldsymbol{x}$ and $g(\boldsymbol{x})$ are guaranteed to be consistently transformed by the same formula $T(\bullet\mid\boldsymbol{\theta}^*)$ and can be

used for the following reliability analysis. When the analytical formula of the auxiliary LSF as well as the new probability distribution of $\boldsymbol{z}$ w.r.t. $\boldsymbol{\theta}$ are precisely known, the failure probability value at $\boldsymbol{\theta}$ corresponding to the s th sample can be easily computed.

Actually, an analytical formula of $h^{(s)}(\boldsymbol{z})=0$ can be easily derived based on the hyperplane equation. In n-dimensional space of $\boldsymbol{z}$, the equation of a hyperplane is determined by $\boldsymbol{\omega}^T\boldsymbol{Z}=\beta$, where $\boldsymbol{\omega}=(\omega_1,\cdots,\omega_n)^T$ refers to the normalized unit vector orthogonal to the hyperplane, and β refers to the distance from the origin point to the hyperplane. Hence, when the normalized unit vector and the distance are known, the hyperplane can be uniquely determined. In the classical line sampling, the reliability index $\tilde{c}^{(s)}$ indicates the distance β and the unit important direction $\boldsymbol{e}_\alpha$ represents the normalized unit vector ω. As shown in Fig.3, for each sample $\boldsymbol{z}^{(s)}$, the corresponding hyperplane is orthogonal to the important direction $\boldsymbol{e}_\alpha$, and contains the intersection point $\boldsymbol{z}^{\perp(s)}+\tilde{c}^{(s)}\boldsymbol{e}_\alpha$. Based on the rationale of the first-order reliability method, the failure probability of Eq.(14) actually equals to the probability mass of the failure domain specified by the auxiliary hyperplane. As a consequence, the original failure domain $F_z: h(\boldsymbol{z})\le 0$ can be approximated by a series of hyperplanes orthogonal to the important direction. Thus for the s th line sample, the analytical formula of auxiliary hyperplane is expressed as

$$h^{(s)}(\boldsymbol{z})=\tilde{c}^{(s)}-\boldsymbol{e}_\alpha\boldsymbol{z}=0 \tag{17}$$

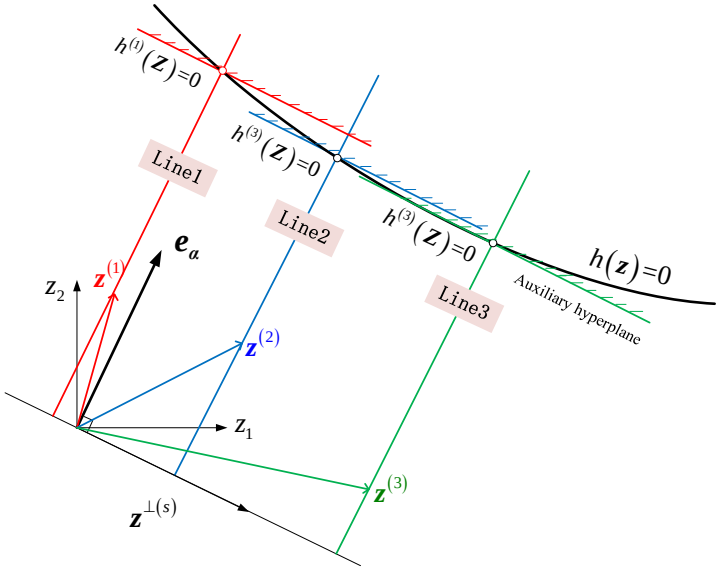

Fig.3 Interpretation of the auxiliary hyperplane for each line sample in standard normal space

As mentioned above, the model structure $h(\boldsymbol{z})$ stays unchanged since the transformation $\boldsymbol{z}=T(\boldsymbol{x}|\boldsymbol{\theta}^*)$ is fixed, and the model structure itself has no relation to the uncertainty characterization of model inputs from a theoretical point of view. In fact, the probability mass of failure domain determined by the established hyperplane will change w.r.t. $\boldsymbol{\theta}$. Hence the approximated formula $h^{(s)}(\boldsymbol{z})$ can be utilized for estimating failure probability function $P_f(\boldsymbol{\theta})$ by averaging the failure

probability function $P_f^{(s)}(\boldsymbol{\theta})$ across all hyperplanes.

$P_f^{(s)}(\boldsymbol{\theta})$ can be estimated by using reliability index, for imprecise variables, the new reliability index becomes a function of $\boldsymbol{\theta}$, denoted by $c^{(s)}(\boldsymbol{\theta})$. If $h^{(s)}(\boldsymbol{z})$ follows Gaussian distribution, the definition of reliability index can be expressed as

$$c^{(s)}(\boldsymbol{\theta}) = \frac{\mu_{h^{(s)}}(\boldsymbol{\theta})}{\sigma_{h^{(s)}}(\boldsymbol{\theta})} = \frac{\tilde{c}^{(s)} - \sum_{d=1}^{n} e_{\boldsymbol{\alpha},d}\,\mu_{z_d}(\boldsymbol{\theta})}{\sqrt{\sum_{d=1}^{n} {e_{\boldsymbol{\alpha},d}}^2 \sigma_{z_d}^2(\boldsymbol{\theta})}} \tag{18}$$

where $e_{\boldsymbol{\alpha},d}$ is the d th element in $\boldsymbol{e}_{\boldsymbol{\alpha}}$, $\mu_{z_d}(\boldsymbol{\theta})$ and $\sigma_{z_d}(\boldsymbol{\theta})$ refer to the renewed mean and standard deviation of z_d corresponding to the new value $\boldsymbol{\theta}$ (the derivation of renewed mean and standard variation will be discussed later). Specifically, when $\boldsymbol{\theta}=\boldsymbol{\theta}^*$, $\mu_{z_d}=0$, $\sigma_{z_d}=1$ and $c^{(s)}(\boldsymbol{\theta})=\tilde{c}^{(s)}$. Then the estimator of $P_f(\boldsymbol{\theta})$ is as follows,

$$\hat{P}_f(\boldsymbol{\theta}) = \frac{1}{N}\sum_{s=1}^{N} P_f^{(s)}(\boldsymbol{\theta}) = \frac{1}{N}\sum_{s=1}^{N} \Phi\left(-c^{(s)}(\boldsymbol{\theta})\right) \tag{19}$$

, and the variance of the estimator is

$$Var\left[\hat{P}_f(\boldsymbol{\theta})\right] = \frac{1}{N(N-1)}\sum_{s=1}^{N}\left[\Phi\left(-c^{(s)}(\boldsymbol{\theta})\right) - \hat{P}_f(\boldsymbol{\theta})\right]^2 \tag{20}$$

In the above procedure, we only need to call the LSF when establishing each auxiliary hyperplane, thus the computational cost is the same as that of the classical line sampling. It should be noted that the estimator in Eq.(19) is biased due to the approximation of limit state function through auxiliary hyperplane, the closer $\boldsymbol{\theta}$ is to $\boldsymbol{\theta}^*$, the less biased the estimator will be.

Based on the rationale of NISS reviewed in subsection 2.1, Eq.(19) can be further decomposed with the cut-HDMR, and the estimators of the first two order components are derived as

$$\begin{cases} \hat{P}_{f0} = \dfrac{1}{N}\sum_{s=1}^{N} \Phi\left(-\tilde{c}^{(s)}\right) \\ \hat{P}_{fi}(\theta_i) = \dfrac{1}{N}\sum_{s=1}^{N}\left(\Phi\left(-c^{(s)}(\theta_i, \boldsymbol{\theta}^*_{-i})\right) - \Phi\left(-\tilde{c}^{(s)}\right)\right) \\ \hat{P}_{fij}(\theta_i, \theta_j) = \dfrac{1}{N}\sum_{s=1}^{N}\left(\Phi\left(-c^{(s)}(\theta_i, \theta_j, \boldsymbol{\theta}^*_{-i,j})\right) - \Phi\left(-c^{(s)}(\theta_i, \boldsymbol{\theta}^*_{-i})\right) - \Phi\left(-c^{(s)}(\theta_j, \boldsymbol{\theta}^*_{-j})\right) + \Phi\left(-\tilde{c}^{(s)}\right)\right) \end{cases} \tag{21}$$

where $c^{(s)}(\theta_i, \boldsymbol{\theta}^*_{-i})$ and $c^{(s)}(\theta_i, \theta_j, \boldsymbol{\theta}^*_{-i,j})$ indicate the first-order and second-order reliability index functions, respectively. Note that those reliability index functions can be easily derived by Eq.(18), therefore, the component functions can also analytically derived with no additional limit function evaluations. The statistical error due to Monte Carlo simulation, which is also a function of $\boldsymbol{\theta}$, can be estimated by the variances of the estimators derived as:

$$\begin{cases} Var\left(\hat{P}_{f0}\right)=\dfrac{1}{N\left(N-1\right)}\sum_{s=1}^{N}\left(\Phi\left(-\tilde{c}^{(s)}\right)-\hat{P}_{f0}\right)^2 \\ Var\left(\hat{P}_{fi}\right)=\dfrac{1}{N\left(N-1\right)}\sum_{s=1}^{N}\left(\Phi\left(-c^{(s)}\left(\theta_i,\boldsymbol{\theta}_{-i}^{*}\right)\right)-\Phi\left(-\tilde{c}^{(s)}\right)-\hat{P}_{fi}\right)^2 \\ Var\left(\hat{P}_{fij}\right)=\dfrac{1}{N\left(N-1\right)}\sum_{s=1}^{N}\left(\Phi\left(-c^{(s)}\left(\theta_i,\theta_j,\boldsymbol{\theta}_{-i,j}^{*}\right)\right)-\Phi\left(-c^{(s)}\left(\theta_i,\boldsymbol{\theta}_{-i}^{*}\right)\right)-\Phi\left(-c^{(s)}\left(\theta_j,\boldsymbol{\theta}_{-j}^{*}\right)\right)+\Phi\left(-\tilde{c}^{(s)}\right)-\hat{P}_{fij}\right)^2 \end{cases} \tag{22}$$

With those explicit component functions, parametric sensitivity analysis can be applied based on the definition in Eq.(9). The above procedure solves imprecise reliability problems by the auxiliary hyperplane approximation of failure boundary, thus is denoted by hyperplane-approximation based approach.

Note that the accuracy of reliability index function given in Eq.(18) depends on the distribution type of input variables. For normal and lognormal distributions, $h^{(s)}\left(\boldsymbol{z}\right)$ follows the Gaussian distribution, then the definition in Eq.(18) is accurate. However, for other distribution types, a change of $\boldsymbol{\theta}$ may result to a non-Gaussian distribution of $h^{(s)}\left(\boldsymbol{z}\right)$, then this definition is not accurate anymore. A more detailed discussion about this is given below with normal, lognormal and general cases, separately.

(1) Normal distribution

First, we discuss the analytical formulation of the renewed mean function $\mu_{z_d}\left(\boldsymbol{\theta}\right)$ and variance function $\sigma_{z_d}^2\left(\boldsymbol{\theta}\right)$ utilized in Eq.(18). For normal variable x_d, the chosen distribution parameters $\boldsymbol{\theta}_d^*$ are specified as μ_d^* and σ_d^*, the varying parameters $\boldsymbol{\theta}_d$ are specified as μ_d and σ_d, the transformation formula is then specified as $T\left(x_d\,|\,\boldsymbol{\theta}_d^*\right)=\left(x_d-\mu_d^*\right)\big/\sigma_d^*=z_d$. Then z_d is regarded as a linear transformation of x_d, it is obvious that z_d still follows normal distribution with mean parameter $\mu_{z_d}\left(\mu_d\right)=E\left(z_d\right)=\left(\mu_d-\mu_d^*\right)\big/\sigma_d^*$ and standard deviation parameter $\sigma_{z_d}\left(\sigma_d\right)=\sqrt{Var\left(z_d\right)}=\sigma_d\big/\sigma_d^*$, where $E\left(\bullet\right)$ and $Var\left(\bullet\right)$ represent the expectation and variance operators respectively.

For simplification, when all input variables follow normal distribution, the analytical expression of first-order reliability indices $c^{(s)}\left(\theta_i,\boldsymbol{\theta}_{-i}^{*}\right)$ w.r.t. μ_i and σ_i in Eq.(21) can be derived as

$$\begin{cases} c^{(s)}\left(\mu_i\right)=\tilde{c}^{(s)}-e_{\alpha,i}\dfrac{\left(\mu_i-\mu_i^*\right)}{\sigma_i^*} \\ c^{(s)}\left(\sigma_i\right)=\dfrac{\tilde{c}^{(s)}}{\sqrt{e_{\alpha,i}{}^2\dfrac{\sigma_i{}^2}{\sigma_i^{*2}}+\sum_{d=1,d\neq i}^{n}e_{\alpha,d}{}^2}} \end{cases} \tag{23}$$

The second-order reliability index $c^{(s)}\left(\theta_i,\theta_j,\boldsymbol{\theta}_{-i,j}^{*}\right)$ in Eq.(21) is expressed as

$$\begin{cases} c^{(s)}\left(\mu_i,\mu_j\right)=\tilde{c}^{(s)}-e_{\boldsymbol{\alpha},i}\dfrac{\left(\mu_i-\mu_i^*\right)}{\sigma_i^*}-e_{\boldsymbol{\alpha},j}\dfrac{\left(\mu_j-\mu_j^*\right)}{\sigma_j^*}\ \ (i\neq j) \\ c^{(s)}\left(\sigma_i,\sigma_j\right)=\dfrac{\tilde{c}^{(s)}}{\sqrt{{e_{\boldsymbol{\alpha},i}}^2\dfrac{{\sigma_i}^2}{{\sigma_i^*}^2}+{e_{\boldsymbol{\alpha},j}}^2\dfrac{{\sigma_j}^2}{{\sigma_j^*}^2}+\sum_{\substack{d=1\\ d\neq i,d\neq j}}^{n}{e_{\boldsymbol{\alpha},d}}^2}} \\ c^{(s)}\left(\mu_i,\sigma_j\right)=\dfrac{\tilde{c}^{(s)}-e_{\boldsymbol{\alpha},i}\dfrac{\left(\mu_i-\mu_i^*\right)}{\sigma_i^*}}{\sqrt{{e_{\boldsymbol{\alpha},j}}^2\dfrac{{\sigma_j}^2}{{\sigma_j^*}^2}+\sum_{d=1,d\neq j}^{n}{e_{\boldsymbol{\alpha},d}}^2}} \end{cases} \tag{24}$$

The estimators of the component failure probability functions are then accordingly specified. For example, $\hat{P}_{fi}\left(\mu_i\right)=\dfrac{1}{N}\sum_{s=1}^{N}\left(\Phi\left(e_{\boldsymbol{\alpha},i}\dfrac{\left(\mu_i-\mu_i^*\right)}{\sigma_i^*}-\tilde{c}^{(s)}\right)-\Phi\left(-\tilde{c}^{(s)}\right)\right)$.

(2) Lognormal distribution

For lognormal distribution $x_d\sim\log N\left(\mu_d,\sigma_d^2\right)$, the PDF of x_d is known as

$$f\left(x_d\right)=\frac{1}{\sigma_d x_d\sqrt{2\pi}}e^{-\frac{\left(\ln x_d-\mu_d\right)^2}{2\sigma_d^2}} \tag{25}$$

where μ_d and σ_d are the expected value and standard deviation of the normal distribution associated with x_d. The mean value and variance of x_d are calculated as $m=e^{\mu_d+\frac{\sigma_d^2}{2}}$, and $v=\left(e^{\sigma_d^2}-1\right)e^{2\mu_d+\sigma_d^2}$, respectively. The transformation formula is specified as $T\left(x_d\,|\,\boldsymbol{\theta}_d^*\right)=\left(\ln x_d-\mu_d^*\right)/\sigma_d^*=z_d$. z_d can be regarded as a linear transformation of $\ln x_d$, and as $\ln x_d$ is following normal distribution $N\left(\mu_d,\sigma_d^2\right)$, then z_d also follows normal distribution with its mean and standard variance as $\mu_{z_d}\left(\mu_d\right)=\left(\mu_d-\mu_d^*\right)/\sigma_d^*$ and $\sigma_{z_d}\left(\sigma_d\right)=\sigma_d/\sigma_d^*$, respectively. The formulas of renewed mean and standard variance are actually the same with the case of normal distribution type. As a consequence, the subsequent procedure of estimating failure probability function is also the same. Since the approximated LSF $h^{(s)}\left(\boldsymbol{z}\right)$ is a linear combination of $\boldsymbol{z}$, thus it follows a Gaussian distribution for normal and lognormal input variables.

(3) General case

When x_d follows general distribution types with the PDF $f_{X_d}\left(x_d\,|\,\boldsymbol{\theta}_d\right)$, the translation formula is $T\left(x_d\,|\,\boldsymbol{\theta}_d^*\right)=\Phi^{-1}\left(F_{X_d}\left(x_d|\boldsymbol{\theta}_d^*\right)\right)=z_d$. For general case, z_d might be non-Gaussian distribution, we propose to do classical Monte Carlo simulation to estimate $P_f\left(\boldsymbol{\theta}\right)$ instead of using reliability index. For any value of $\boldsymbol{\theta}$, generating M samples $\left(x_1^{(r)},\cdots,x_n^{(r)}\right)\left(r=1,\cdots,M\right)$, then evaluating the corresponding samples $\left(z_1^{(r)},\cdots,z_n^{(r)}\right)\left(r=1,\cdots,M\right)$ by using transformation formula. Then failure

probability can be easily estimated as

$$P_f^{(s)} = \frac{1}{M}\sum_{r=1}^{M} h^{(s)}\left(\boldsymbol{z}^{(r)}\right) = \frac{1}{M}\sum_{r=1}^{M}\left(\tilde{c}^{(s)} - \boldsymbol{e}_\alpha \boldsymbol{z}^{(r)}\right) \tag{26}$$

Although it requires resampling for each $\boldsymbol{\theta}$ value, but it will not require additional evaluation of real LSF since the formula $h^{(s)}(\boldsymbol{z})$ is analytically known. And the following steps for estimating $P_f(\boldsymbol{\theta})$ are the same as those with the case of normal distribution. Note that for dependent input variables, it is also necessary to firstly transform the input variables from correlated distribution space into standard Gaussian space, then the residual procedures will be almost the same with the independent case.

3.2 Weighted-integral based imprecise line sampling

In this subsection, we develop another strategy based on the formula of line sampling integral, denoted as weighted-integral ILS (WI-ILS), for injecting the line sampling into the NISS framework.

Like HA-ILS method, the first step of WI-ILS is also to perform the classical line sampling method for the constant cut-HDMR component with the distribution parameters $\boldsymbol{\theta}$ being fixed at $\boldsymbol{\theta}^*$, and all the following discussions and developments are based on the standard normal space obtained by the fixed transformation $\boldsymbol{z}=T(\boldsymbol{x}\,|\,\boldsymbol{\theta}^*)$. By differentiating both sides of $\Phi(\boldsymbol{z})=F_X(\boldsymbol{x}|\boldsymbol{\theta}^*)$, one can obtain $\phi(\boldsymbol{z})\mathrm{d}\boldsymbol{z}=f_X(\boldsymbol{x}\,|\,\boldsymbol{\theta}^*)\mathrm{d}\boldsymbol{x}$. Thus the integral of failure probability function in Eq.(2) can be rewritten as

$$P_f(\boldsymbol{\theta}) = \int_{g(x)\le 0} \frac{f_X(\boldsymbol{x}\,|\,\boldsymbol{\theta})}{f_X(\boldsymbol{x}\,|\,\boldsymbol{\theta}^*)} f_X(\boldsymbol{x}\,|\,\boldsymbol{\theta}^*)\mathrm{d}\boldsymbol{x} = \int_{g\left(T^{-1}(\boldsymbol{z}\,|\,\boldsymbol{\theta}^*)\right)\le 0} \frac{f_X\left(T^{-1}(\boldsymbol{z}\,|\,\boldsymbol{\theta}^*)\,|\,\boldsymbol{\theta}\right)}{f_X\left(T^{-1}(\boldsymbol{z}\,|\,\boldsymbol{\theta}^*)\,|\,\boldsymbol{\theta}^*\right)}\phi(\boldsymbol{z})\mathrm{d}\boldsymbol{z} \tag{27}$$

Based on the rationale of line sampling, decomposing $\boldsymbol{z}$ as $\boldsymbol{z}=\boldsymbol{z}^{\perp}+\bar{z}\boldsymbol{e}_\alpha$ can reshape the *n*-dimensional integral of Eq.(27) orthogonally into a double-loop integral, where the outer loop is a (*n*-1)-dimensional integral in the space of $\boldsymbol{z}^{\perp}$, and the inner loop is a one-dimensional integral in the space of $\bar{z}$, thus $P_f(\boldsymbol{\theta})$ can be expressed as

$$P_f(\boldsymbol{\theta}) = \int_{g\left(T^{-1}\left(\boldsymbol{z}^{\perp}+\bar{z}\boldsymbol{e}_\alpha\,|\,\boldsymbol{\theta}^*\right)\right)\le 0} \eta\left(\boldsymbol{z}^{\perp}+\bar{z}\boldsymbol{e}_\alpha,\boldsymbol{\theta},\boldsymbol{\theta}^*\right)\phi(\bar{z})\mathrm{d}\bar{z}\,\phi\left(\boldsymbol{z}^{\perp}\right)\mathrm{d}\boldsymbol{z}^{\perp} \tag{28}$$

where $\eta\left(\boldsymbol{z}^{\perp}+\bar{z}\boldsymbol{e}_\alpha,\boldsymbol{\theta},\boldsymbol{\theta}^*\right)$ denotes the PDF weight, and is expressed as

$$\eta\left(\boldsymbol{z}^{\perp}+\bar{z}\boldsymbol{e}_\alpha,\boldsymbol{\theta},\boldsymbol{\theta}^*\right) = \frac{f_X\left(T^{-1}\left(\boldsymbol{z}^{\perp}+\bar{z}\boldsymbol{e}_\alpha\,|\,\boldsymbol{\theta}^*\right)\,|\,\boldsymbol{\theta}\right)}{f_X\left(T^{-1}\left(\boldsymbol{z}^{\perp}+\bar{z}\boldsymbol{e}_\alpha\,|\,\boldsymbol{\theta}^*\right)\,|\,\boldsymbol{\theta}^*\right)} \tag{29}$$

With the set of samples of $\boldsymbol{z}^{\perp(s)}$ $(s=1,\cdots,N)$ following (*n*-1)-dimensional PDF $\phi\left(\boldsymbol{z}^{\perp}\right)$, the estimator of $P_f(\boldsymbol{\theta})$ is derived as:

$$\hat{P}_f(\boldsymbol{\theta}) = \frac{1}{N}\sum_{s=1}^{N}\int_{g\left(T^{-1}\left(\boldsymbol{z}^{\perp(s)}+\bar{z}\boldsymbol{e}_\alpha\,|\,\boldsymbol{\theta}^*\right)\right)\le 0} \eta\left(\boldsymbol{z}^{\perp(s)}+\bar{z}\boldsymbol{e}_\alpha,\boldsymbol{\theta},\boldsymbol{\theta}^*\right)\phi(\bar{z})\mathrm{d}\bar{z} \tag{30}$$

Note that the one-dimensional failure domain defined by $g\left(T^{-1}\left(\boldsymbol{z}^{\perp(s)}+\bar{z}\boldsymbol{e}_\alpha\,|\,\boldsymbol{\theta}^*\right)\right)\le 0$ is actually the same failure domain along the line $l^{(s)}(\bar{z},\boldsymbol{e}_\alpha)$ which has been discussed in section 2.2. Hence, the

integral boundary can be replaced by $[\tilde{c}^{(s)},+\infty)$, where $\tilde{c}^{(s)}$ corresponds to the intersection point between the line and limit state boundary. Let $L^{(s)}(\boldsymbol{\theta})$ denote the integral in Eq.(30) as

$$L^{(s)}(\boldsymbol{\theta})=\int_{\tilde{c}^{(s)}}^{\infty}\eta\left(\boldsymbol{z}^{\perp(s)}+\bar{z}\boldsymbol{e}_{\alpha},\boldsymbol{\theta},\boldsymbol{\theta}^{*}\right)\phi(\bar{z})\mathrm{d}\bar{z} \tag{31}$$

Specifically, when $\boldsymbol{\theta}=\boldsymbol{\theta}^{*}$, $\eta=1$ and $L^{(s)}(\boldsymbol{\theta})=\Phi\left(-\tilde{c}^{(s)}\right)$. Thus the estimator of failure probability function can be represented as

$$\hat{P}_f(\boldsymbol{\theta})=\frac{1}{N}\sum_{s=1}^{N}L^{(s)}(\boldsymbol{\theta}) \tag{32}$$

Similar with the HA-ILS method in subsection 3.1 (see Eq.(20)-(22)), the variance of the above estimator, the estimator of cut-HDMR component functions as well as the variance of each component can be easily derived, which is omitted here. Actually, the computation of Eq.(31) does not require any additional performance function evaluations, thus making it possible that the computational cost of line sampling for the estimation of $P_f(\boldsymbol{\theta})$ is the same with $P_f\left(\boldsymbol{\theta}^{*}\right)$. Note that, all the expressions above can be easily evaluated through one-dimensional numerical integration and do not involve any other approximations.

Now the main problem is to estimate the value of integral $L^{(s)}(\boldsymbol{\theta})$, which can be derived analytically for some specific distribution types, and a detailed discussion is given below.

(1) Normal distribution

For the d th variable, $X_d\sim N\left(\mu_d,\sigma_d^2\right)$, and $x_d=T^{-1}\left(z_d\,|\boldsymbol{\theta}_d^{*}\right)$ can be specified as

$$x_d=\mu_d^{*}+\sigma_d^{*}z_d=\mu_d^{*}+\sigma_d^{*}z_d^{\perp(s)}+\sigma_d^{*}\bar{z}e_{\alpha,d} \tag{33}$$

Then the PDF weight in Eq.(29) can be derived analytically as

$$\eta=\left(\prod_{d=1}^{n}\frac{\sigma_d^{*}}{\sigma_d}\right)\exp\left(\sum_{d=1}^{n}\left(\frac{\left(\mu_d^{*}+\sigma_d^{*}z_d^{\perp(s)}+\sigma_d^{*}\bar{z}e_{\alpha,d}-\mu_d^{*}\right)^2}{2\sigma_d^{*2}}-\frac{\left(\mu_d^{*}+\sigma_d^{*}z_d^{\perp(s)}+\sigma_d^{*}\bar{z}e_{\alpha,d}-\mu_d\right)^2}{2\sigma_d^{2}}\right)\right) \tag{34}$$

Then substituting Eq.(34) into Eq.(31) analytically, the integral is expressed as

$$L^{(s)}(\boldsymbol{\mu},\boldsymbol{\sigma})==\frac{\xi}{\sqrt{1-2\zeta}}\exp\left(\lambda^{(s)}+\frac{\left(\kappa^{(s)}\right)^2}{2-4\zeta}\right)\Phi\left(\frac{\kappa^{(s)}-(1-2\zeta)c^{(s)}}{\sqrt{1-2\zeta}}\right) \tag{35}$$

One can refer to **Appendix A** for detailed definition of parameters ξ, ζ, $\lambda^{(s)}$, $\kappa^{(s)}$, as well as the derivations of the analytical formula in Eq.(35). After that, the estimator of failure probability function and the corresponding variance of estimator can be derived accordingly.

Furtherly, the first-order and second-order failure probability functions can be derived with cut-HDMR decomposition, and the integral functions in $P_f\left(\theta_i,\boldsymbol{\theta}_{-i}^{*}\right)$ and $P_f\left(\theta_i,\theta_j,\boldsymbol{\theta}_{-i,j}^{*}\right)$ are denoted by $L^{(s)}(\mu_i)$, $L^{(s)}\left(\mu_j\right)$, $L^{(s)}\left(\mu_i,\mu_j\right)$, $L^{(s)}\left(\sigma_i,\sigma_j\right)$, $L^{(s)}\left(\mu_i,\sigma_j\right)$, respectively. The corresponding self-defined parameters ξ, ζ, $\lambda^{(s)}$, $\kappa^{(s)}$ within integral functions are given in Table 1.

Table 1 Analytical expressions of parameters ξ, ζ, $\lambda^{(s)}$, $\kappa^{(s)}$ in component integral functions

Integral functions	ξ	ζ	$\lambda^{(s)}$	$\kappa^{(s)}$
$L^{(s)}(\mu_i)$	1	0	$\frac{\left(z_i^{\perp(s)}\right)^2}{2}-\frac{\left(\mu_i^*+\sigma_i^* z_i^{\perp(s)}-\mu_i\right)^2}{2\sigma_i^{*2}}$	$\frac{\left(\mu_i-\mu_i^*\right)e_{\alpha,i}}{\sigma_i^*}$
$L^{(s)}(\sigma_i)$	$\frac{\sigma_i^*}{\sigma_i}$	$\frac{e_{\alpha,i}^2}{2}\left(1-\frac{\sigma_i^{*2}}{\sigma_i^2}\right)$	$\frac{\left(z_i^{\perp(s)}\right)^2}{2}\left(1-\frac{\sigma_i^{*2}}{\sigma_i^2}\right)$	$z_i^{\perp(s)}e_{\alpha,i}\left(1-\frac{\sigma_i^{*2}}{\sigma_i^2}\right)$
$L^{(s)}(\mu_i,\mu_j)$	1	0	$\sum_{k=i,j}\frac{\left(z_k^{\perp(s)}\right)^2}{2}-\frac{\left(\mu_k^*+\sigma_k^* z_k^{\perp(s)}-\mu_k\right)^2}{2\sigma_k^{*2}}$	$\sum_{k=i,j}\frac{\left(\mu_k-\mu_k^*\right)e_{\alpha,k}}{\sigma_k^*}$
$L^{(s)}(\sigma_i,\sigma_j)$	$\frac{\sigma_i^*\sigma_j^*}{\sigma_i\sigma_j}$	$\sum_{k=i,j}\left(\frac{e_{\alpha,k}^2}{2}\left(1-\frac{\sigma_k^{*2}}{\sigma_k^2}\right)\right)$	$\sum_{k=i,j}\frac{\left(z_k^{\perp(s)}\right)^2}{2}\left(1-\frac{\sigma_k^{*2}}{\sigma_k^2}\right)$	$\sum_{k=i,j}z_k^{\perp(s)}e_{\alpha,k}\left(1-\frac{\sigma_k^{*2}}{\sigma_k^2}\right)$
$L^{(s)}(\mu_i,\sigma_i)$	$\frac{\sigma_i^*}{\sigma_i}$	$\frac{e_{\alpha,i}^2}{2}\left(1-\frac{\sigma_i^{*2}}{\sigma_i^2}\right)$	$\frac{\left(z_i^{\perp(s)}\right)^2}{2}-\frac{\left(\mu_i^*+\sigma_i^* z_i^{\perp(s)}-\mu_i\right)^2}{2\sigma_i^2}$	$z_i^{\perp(s)}e_{\alpha,i}-\frac{\left(\mu_i^*+\sigma_i^* z_i^{\perp(s)}-\mu_i\right)\sigma_i^* e_{\alpha,i}}{\sigma_i^2}$
$L^{(s)}(\mu_i,\sigma_j)$ $(i\neq j)$	$\frac{\sigma_j^*}{\sigma_j}$	$\frac{e_{\alpha,j}^2}{2}\left(1-\frac{\sigma_j^{*2}}{\sigma_j^2}\right)$	$\frac{\left(z_i^{\perp(s)}\right)^2}{2}-\frac{\left(\mu_i^*+\sigma_i^* z_i^{\perp(s)}-\mu_i\right)^2}{2\sigma_i^{*2}}+\frac{\left(z_j^{\perp(s)}\right)^2}{2}\left(1-\frac{\sigma_j^{*2}}{\sigma_j^2}\right)$	$\frac{\left(\mu_i-\mu_i^*\right)e_{\alpha,i}}{\sigma_i^*}+z_j^{\perp(s)}e_{\alpha,j}\left(1-\frac{\sigma_j^{*2}}{\sigma_j^2}\right)$

(2) Lognormal distribution

For the lognormal type of distribution, the transformation formula is specified as $T\left(\boldsymbol{x}\,|\,\boldsymbol{\theta}^*\right)=\left(\ln x_d-\mu_d^*\right)\big/\sigma_d^*$, decomposing z_d with $z_d=z_d^{\perp(s)}+\overline{z}e_{\alpha,d}$, the relation between x_d and z_d can be expressed as

$$\ln x_d=\mu_d^*+\sigma_d^* z_d^{\perp(s)}+\sigma_d^*\overline{z}e_{\alpha,d} \tag{36}$$

Then the PDF weight η has the following expression

$$\eta=\left(\prod_{d=1}^{n}\frac{\sigma_d^*}{\sigma_d}\right)\exp\left(\sum_{d=1}^{n}\left(\frac{\left(\ln x_d-\mu_d^*\right)^2}{2\sigma_d^{*2}}-\frac{\left(\ln x_d-\mu_d\right)^2}{2\sigma_d^2}\right)\right) \tag{37}$$

Replacing $\ln x_d$ with $\mu_d^*+\sigma_d^* z_d^{\perp(s)}+\sigma_d^*\overline{z}e_{\alpha,d}$, we can find that the analytical expression of η turns out to be completely the same as in Eq.(34), obviously, the following procedure for estimating integral function $L^{(s)}(\boldsymbol{\theta})$ as well as the failure probability functions is also the same as normal distribution type.

(3) General case

When x_d follows general distribution with the PDF $f_{X_d}\left(x_d\,|\,\boldsymbol{\theta}_d\right)$, the relationship between x_d and z_d becomes $x_d=F_{X_d}^{-1}\left(\Phi\left(z_d^{\perp(s)}+\overline{z}e_{\alpha,d}\right)|\boldsymbol{\theta}_d^*\right)$, then PDF weight is

$$\eta=\prod_{d=1}^{n}\frac{f_{X_d}\left(F_{X_d}^{-1}\left(\Phi\left(z_d{}^{\perp(s)}+\bar{z}e_{\alpha,d}\right)|\boldsymbol{\theta}_d{}^{*}\right)|\boldsymbol{\theta}_d\right)}{f_{X_d}\left(F_{X_d}^{-1}\left(\Phi\left(z_d{}^{\perp(s)}+\bar{z}e_{\alpha,d}\right)|\boldsymbol{\theta}_d{}^{*}\right)|\boldsymbol{\theta}_d{}^{*}\right)} \tag{38}$$

And the integral $L^{(s)}(\boldsymbol{\theta})$ is generally expressed as

$$L^{(s)}(\boldsymbol{\theta})=\int_{\tilde{c}^{(s)}}^{\infty}\prod_{d=1}^{n}\frac{f_{X_d}\left(F_{X_d}^{-1}\left(\Phi\left(z_d{}^{\perp(s)}+\bar{z}e_{\alpha,d}\right)|\boldsymbol{\theta}_d{}^{*}\right)|\boldsymbol{\theta}_d\right)}{f_{X_d}\left(F_{X_d}^{-1}\left(\Phi\left(z_d{}^{\perp(s)}+\bar{z}e_{\alpha,d}\right)|\boldsymbol{\theta}_d{}^{*}\right)|\boldsymbol{\theta}_d{}^{*}\right)}\phi(\bar{z})\mathrm{d}\bar{z} \tag{39}$$

The accuracy of the above one-dimensional integral depends on the specific formula of PDF and CDF, of course, the best way is to derive analytically as normal and lognormal. The following steps for estimating $P_f(\boldsymbol{\theta})$ are all the same with the former cases.

4. Case studies

4.1 Analytical example

Consider a simple analytical example where the LSF is a parabola. The expression for the performance function is

$$g(x_1,x_2)=\beta-x_1+\kappa x_2^2 \tag{40}$$

, where $X_1\sim N\left(\mu_1,\sigma_1^2\right)$, $X_2\sim N\left(\mu_2,\sigma_2^2\right)$. The constant β controls the failure probability level and κ controls the degree of nonlinearity of performance function. The failure probability function can be calculated analytically by solving numerically the following one dimensional integral (see Appendix B).

$$P_f(\mu_1,\mu_2,\sigma_1,\sigma_2)=\int_{-\infty}^{+\infty}\Phi\left(-\frac{\beta-\mu_1}{\sigma_1}-\frac{\kappa}{\sigma_1}\left(\mu_2+\sigma_2 z_2\right)^2\right)\phi\left(z_2\right)\mathrm{d}z_2 \tag{41}$$

Let β=3.5 and κ=0.2 such that the failure is a rare event and the failure surface is mildly nonlinear. The imprecisions of distribution parameters are defined by intervals $\mu_1\in[-0.5,0.5]$, $\mu_2\in[-0.5,0.5]$, $\sigma_1\in[0.6,1]$, $\sigma_2\in[0.8,1]$.

The fixed distribution parameters $\boldsymbol{\theta}^{*}$ are chosen to be $\left(\mu_1^{*},\mu_2^{*},\sigma_1^{*},\sigma_2^{*}\right)=(0,0,1,1)$. For this case, it is straightforward to locate the important direction as $\boldsymbol{e}_{\alpha}=(1,0)^T$. Fig.4 shows the plot of the first-order component functions estimated by HA-ILS and WI-ILS methods, together with the analytical results (dented as ANA) for comparison, where 100 lines with a total of 300 times of performance function evaluations are used in both ILS procedures. Fig.4 shows that first-order component functions of μ_1 and σ_1 are accurately estimated by both methods, however, for the component of μ_2 and σ_2, the results generated by WI-ILS is in good agreement with the analytical solutions, but those generated by HA-ILS show some differences. Thus, WI-ILS shows a better performance than HA-ILS in this case. However, it is important to recall that $\boldsymbol{e}_{\alpha}=(1,0)^T$ with the second element equals to zero, indicating that x_2 may not be important for reliability analysis. According to Eq.(17), x_2 is not involved in hyperplane formula, then the parameter change associated

with x_2 will not be detected. However, one should note that this does not mean HA-ILS method is not applicable for this case. In Fig. 4, the orders of magnitude of μ_2 and σ_2 are much smaller than those of μ_1 and σ_1, thus it does not affect considerably the result of the final synthesized estimation of the failure probability function if it fails to capture the non-influential behavior. The sensitivity indices shown in Table 2 can also validate this conclusion.

The first- and second-order sensitivity indices computed by the HA-ILS and WI-ILS methods are listed in Table 2, together with their standard deviations (SDs) computed by on Eq.(22) as well as the analytical results for comparison. It is shown that the results generated by both HA-ILS and WI-ILS methods have good consistency with the analytical results, illustrating the effectiveness of the proposed two methods. All sensitivity indices associated with x_2 are close to zero, indicating the parameters of x_2 are non-influential to failure probability. As a result, the parameters of x_2 can be fixed at any point in the imprecise intervals for subsequent reliability design and optimization. One should note that all the first- and second-order component functions are estimated with one set of samples, and higher-order components can also be estimated by this set of samples.

Next, we slightly modify the setting of the test example. The parabola is rotated 45 degrees anticlockwise and the *g*-function becomes

$$g = 3.5 - \frac{\sqrt{2}}{2}\left(X_1 + X_2\right) + \frac{0.2}{4}\left(X_1 - X_2\right)^2 \tag{42}$$

The uncertainty characterization of each input variable as well as the fixed parameters $\boldsymbol{\theta}^*$ remain the same. The important direction then is calculated to be $\boldsymbol{e}_{\alpha} = \left(\sqrt{2}/2, \sqrt{2}/2\right)^T$. In this case, the reference results are all calculated by double-loop Monte Carlo method (denoted as DL) with the sample size of each inner loop being 10^7.

For this case, the sensitivity indices are displayed in Table 3 and the results of the proposed two methods match well with the reference solutions. Fig.5 displays the plot of first-order component functions. Compared with Fig.4 of the previous case, HA-ILS behaves much better in Fig.5 because the two components in important direction $\boldsymbol{e}_{\alpha}$ become equal. Besides, the plot of HA-ILS w.r.t σ_1 and σ_2 show a small deviation from the reference results when σ_i is far from σ_i^*, although the corresponding SDs are already smaller than WI-ILS. It indicates HA-ILS converges faster but may go to a biased result because of the approximation of LSF. The component functions always equal to zero at the expansion point $\boldsymbol{\theta}^*$ due to the definition of cut-HDMR components. All the first-order component functions are monotonically increasing w.r.t the respective parameters, then all the maximum and minimum values of the first-order component functions locate at the upper and lower bound of imprecise parameters, respectively.

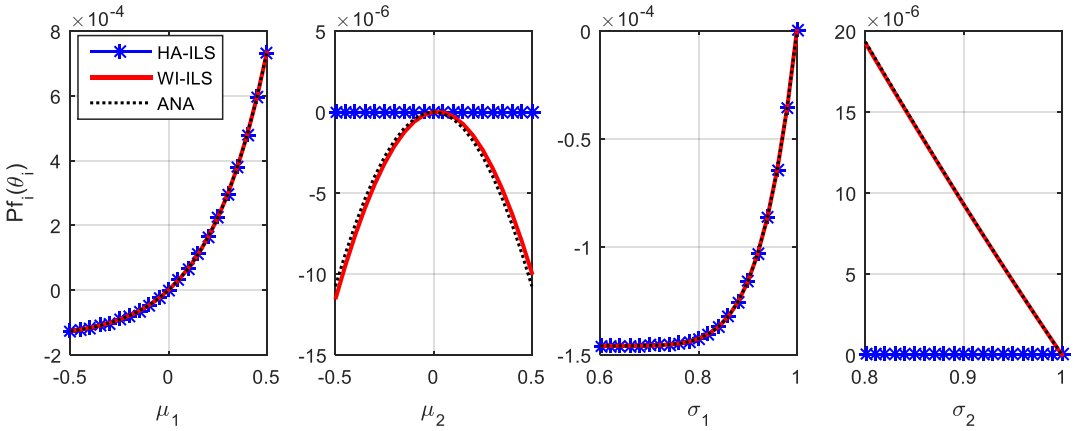

Fig.4 The plot of first-order component functions in the analytical example

Table 2 The first and second order sensitivity indices of the parabolic LSF in the analytical example

Methods		HA-ILS	WI-ILS	ANA
N_{call}		300	300	/
$P_f\left(\theta^*\right)$		1.4585e-4$^{(7.5e-6)}$	1.4585e-4$^{(7.5e-6)}$	1.4584e-4
S_i	μ_1	0.5033$^{(0.0012)}$	0.4866$^{(0.0011)}$	0.5008
	μ_2	0.0000$^{(0.0000)}$	0.0002$^{(4e-5)}$	0.0002
	σ_1	0.1339$^{(0.0003)}$	0.1295$^{(0.0003)}$	0.1332
	σ_2	0.00000$^{(0.0000)}$	0.0009$^{(1e-5)}$	0.0010
S_{ij}	(μ_1,μ_2)	0.0000$^{(0.0001)}$	0.0005$^{(0.0001)}$	0.0005
	(σ_1,σ_2)	0.0000$^{(0.0000)}$	0.0007$^{(1e-5)}$	0.0007
	(μ_1,σ_1)	0.3628$^{(0.0008)}$	0.3790$^{(0.0008)}$	0.3609
	(μ_1,σ_2)	0.0000$^{(0.0000)}$	0.0024$^{(4e-5)}$	0.0025
	(μ_2,σ_1)	0.0000$^{(0.0000)}$	0.0001$^{(3e-5)}$	0.0001
	(μ_2,σ_2)	0.0000$^{(0.0000)}$	0.0000$^{(0.0000)}$	0.0000

Table 3 The sensitivity indices after rotation of the parabola LSF in the analytical example

Methods		HA-ILS	WI-ILS	DL
N_{call}		300	300	/
$P_f\left(\theta^*\right)$		1.7457e-4$^{(6.1e-6)}$	1.7457e-4$^{(6.1e-6)}$	1.7450e-4
S_i	μ_1	0.2012$^{(0.0002)}$	0.1742$^{(0.0003)}$	0.1912
	μ_2	0.2012$^{(0.0002)}$	0.1842$^{(0.0003)}$	0.1898
	σ_1	0.1102$^{(0.0000)}$	0.1086$^{(0.0001)}$	0.1148
	σ_2	0.0556$^{(0.0000)}$	0.0557$^{(0.0001)}$	0.0573
S_{ij}	(μ_1,μ_2)	0.1425$^{(0.0001)}$	0.1414$^{(0.0002)}$	0.1486
	(σ_1,σ_2)	0.0263$^{(0.0000)}$	0.0295$^{(0.0001)}$	0.0308
	(μ_1,σ_1)	0.0905$^{(0.0001)}$	0.1040$^{(0.0002)}$	0.0860
	(μ_1,σ_2)	0.0410$^{(0.0000)}$	0.0437$^{(0.0001)}$	0.0469
	(μ_2,σ_1)	0.0905$^{(0.0001)}$	0.0965$^{(0.0001)}$	0.0999
	(μ_2,σ_2)	0.0410$^{(0.0000)}$	0.0610$^{(0.0002)}$	0.0347

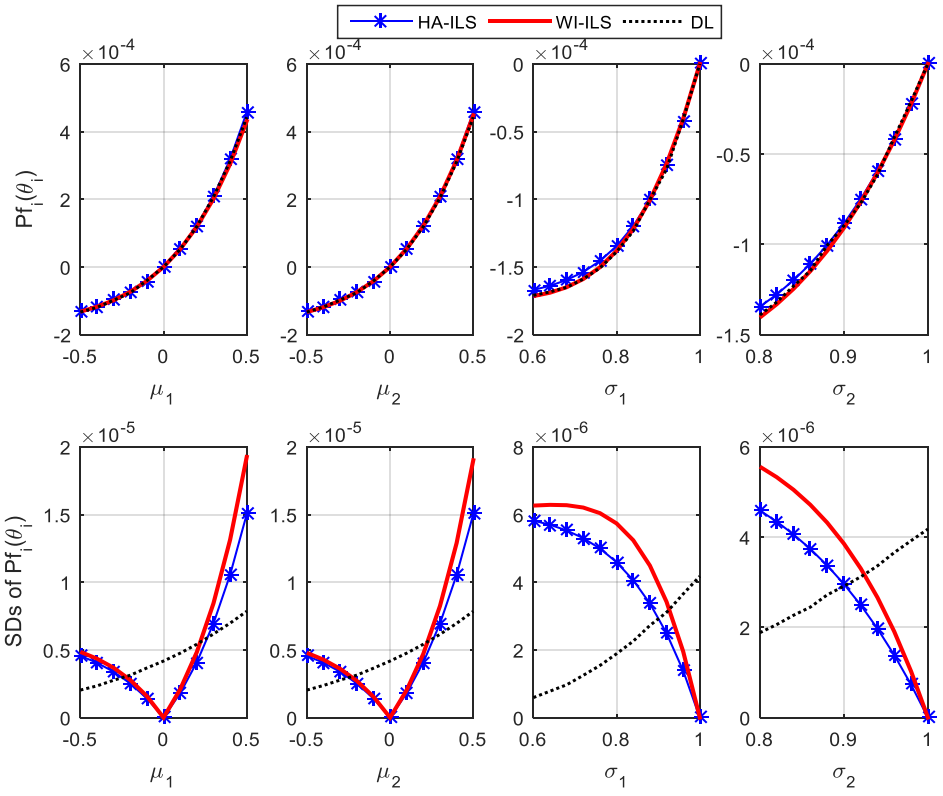

Fig.5 The plot of first-order component functions after rotation of the parabola LSF in the analytical example

4.2 A shallow foundation model

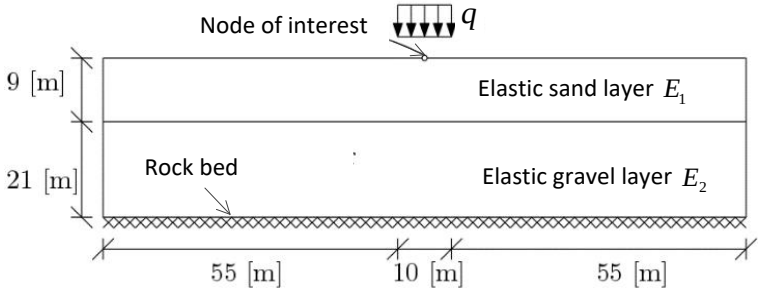

Fig.6 The schematic representation of elastic soil layer of shallow foundation model

Table 4 Distribution parameters of input variables for shallow foundation model

Variables	Description	Distribution type	Mean	c.o.v.
E_1 [kPa]	Young's modulus of sand layer	Lognormal	[27000,33000]	10%
E_2 [kPa]	Young's modulus of gravel layer	Lognormal	[90000,110000]	10%
q [kPa]	Load density	Lognormal	[90,110]	10%

To illustrate the effectiveness of the proposed method to engineering applications, a shallow foundation resting over elastic soil is considered [32], and a finite element model considering of 320 quadrilateral elements is established for simulating the structure [3]. The schematic representation is shown in Fig.6. The elastic soil is composed of two layers. The first layer is a sand layer of 9 [m] thickness while the second is a gravel layer of 21 [m] thickness resting over a rock bed which is assumed as infinitely rigid.

The Young's modulus of the sand and gravel layers are characterized by random variables obeying lognormal distribution, denoted as E_1 and E_2, respectively. The shallow foundation of 10 [m] width applies a distributed load q of over the elastic soil layer. The load intensity q is characterized by means of a lognormal variable as well. The mean value (denoted by m_{E_1}, m_{E_2} and m_q) of the three random variables are imprecisely known varying within intervals, and the c.o.v. (coefficient of variance) are all assumed to be 0.1, as given in Table 4, thus three mean value are modeled as imprecise parameters. The performance function is defined as the threshold level b=0.055 [m] minus the vertical displacement at the center of the shallow foundation.

The expansion point $\boldsymbol{\theta}^*$ are chosen to be $\left(E_1^*, E_2^*, q^*\right) = \left(30000, 100000, 100\right)\left[\text{kPa}\right]$, the important direction is $\boldsymbol{e}_\alpha = \left(-0.6270, -0.1394, , 0.7664\right)^T$ by implementing AFOSM method in standard normal space with 42 times of model evaluation. We firstly plot the components for the failure probability function with the proposed HA-ILS and WI-ILS procedure in which 100 lines with a total of 342 times of model evaluations are involved, as shown in Fig. 7. Since the finite element model of shallow foundation is not very cost-demanding, DL method is also plotted as reference results with $N = 10^6$ for each failure probability evaluation. It shows that the results of both HA-ILS and WI-ILS match well with DL method except that the plot of m_{E_2} by WI-ILS has a slight difference with the

reference results. The plots of HA-ILS keep quite close to the reference plots within the whole range of parameters, showing that not too much bias is introduced by LSF approximations when the values of parameters move away from the expansion point. This indicates that the real LSF of the shallow foundation model may be approximately linear. The plot of SDs shows HA-ILS converges much faster than WI-ILS; specifically, when the value of m_{E_1} is close to the lower bound 27000, the SD of WI-ILS increases sharply while SD of HA-ILS stays at a low value, that means when the values of parameters are far away from the expansion point, HA-ILS shows a much better performance. On the other hand, all the component values vary monotonous with the corresponding parameters, furtherly, it is incremental for q and diminishing for E_1 and E_2.

The sensitivity indices estimated by HA-ILS and WI-ILS are listed in Table 5, as well as the value of constant component $P_f\left(\theta^*\right)$. Among the first-order components, m_{E_1} and m_q are much more influential than m_{E_2}, and among all orders of components, $\left(m_{E_1}, m_q\right)$ is the most influential one, indicating that the interaction effect of m_{E_1} and m_q contributes most to failure probability of shallow foundation model. Note that the third-order index is also estimated in Table 5 with the value less than 0.02, that means the third-order component in non-influential in estimating $P_f(\boldsymbol{\theta})$, so truncation up to second order will not introduce significant errors. Fig.8 shows the 3D plot of the most influential second-order component function $P_{fij}\left(m_{E_1}, m_q\right)$ as well as its SDs by the proposed two methods. In Fig.8 the second-order plots by both methods match well with each other, and the SDs show that WI-ILS converges slower than HA-ILS especially in those points far away from $\boldsymbol{\theta}^*$. The maximum value of $P_{fij}\left(m_{E_1}, m_q\right)$ locates in $\left(2.7\times10^4, 110\right)$, which is also the maximum point of the corresponding first-order plot shown in Fig.7.

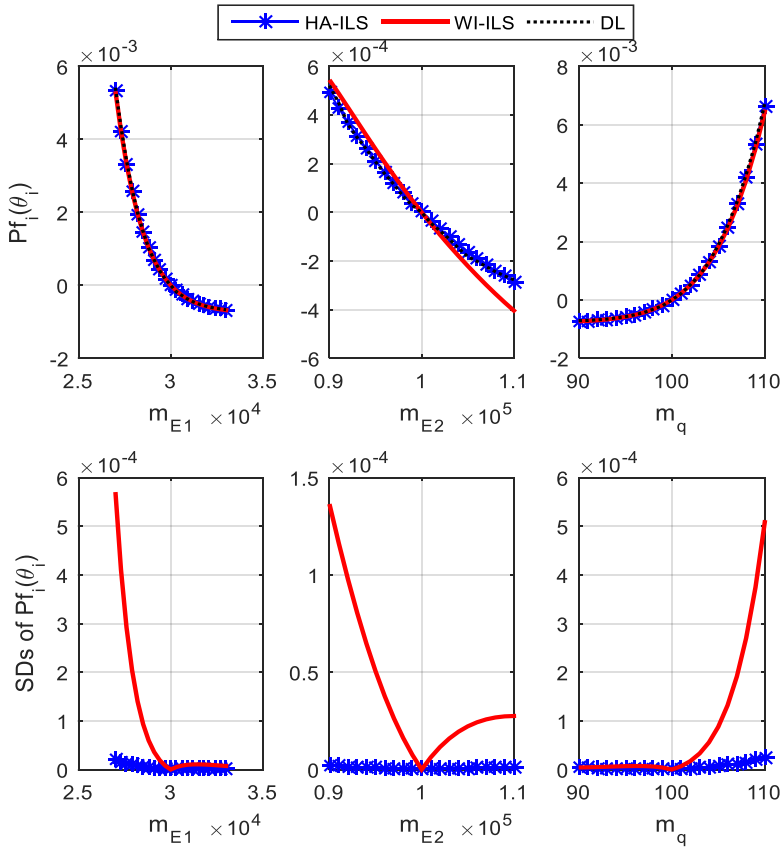

Fig.7 The plot of first-order component functions for shallow foundation model

Table 5 Sensitivity indices for shallow foundation model

Methods		HA-ILS	WI-ILS
N_{call}		342	342
$P_f\left(\theta^*\right)$		7.6609e-4$^{(2.4e-6)}$	7.6609e-4$^{(2.4e-6)}$
S_i	m_{E_1}	0.1732$^{(1e-6)}$	0.1815$^{(0.0006)}$
	m_{E_2}	0.0028$^{(2e-7)}$	0.0025$^{(0.0001)}$
	m_q	0.2341$^{(1e-6)}$	0.2173$^{(0.0005)}$
S_{ij}	$\left(m_{E_1}, m_{E_2}\right)$	0.0101$^{(5e-8)}$	0.0094$^{(0.0010)}$
	$\left(m_{E_1}, m_q\right)$	0.5489$^{(2e-6)}$	0.5558$^{(0.0005)}$
	$\left(m_{E_2}, m_q\right)$	0.0133$^{(6e-8)}$	0.0162$^{(0.0008)}$
S_{ijk}	$\left(m_{E_1}, m_{E_2}, m_q\right)$	0.0175$^{(2e-8)}$	0.0173$^{(0.0014)}$

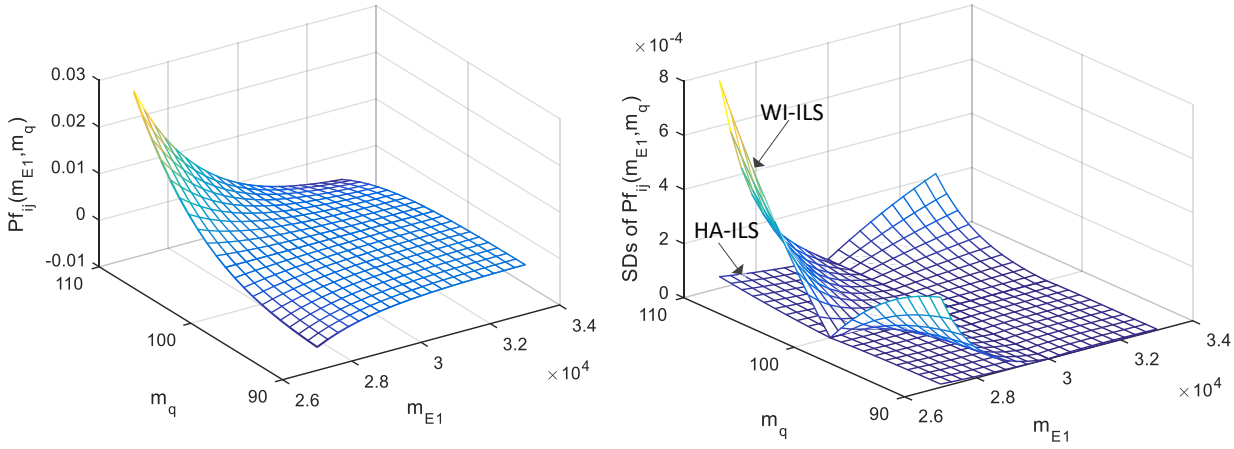

Fig.8 The plot of the most influential second-order component function with both HA-ILS and WI-ILS for shallow foundation model

4.3 Confined seepage model

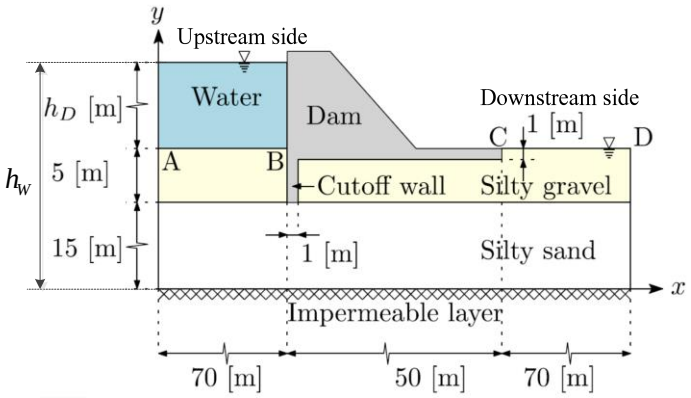

Fig.9 The elevation of the dam in confined seepage model

Table 6 Distribution parameters of input variables for confined seepage model

Inputs	Description	Distribution type	Means	c.o.v.	Bounds
$k_{xx,1}$ [10^{-7}m/s]	Horizontal permeability of sand soil layer	Lognormal	[4.5,5.5]	100%	/
$k_{yy,1}$ [10^{-7}m/s]	Vertical permeability of sand soil layer	Lognormal	[1.8,2.2]	100%	/
$k_{xx,2}$ [10^{-6}m/s]	Horizontal permeability of gravel soil layer	Lognormal	[4.5,5.5]	100%	/
$k_{yy,2}$ [10^{-6}m/s]	Vertical permeability of gravel soil layer	Lognormal	[1.8,2.2]	100%	/
h_D [m]	water height in upstream side of dam	Uniform	/	/	[7,10]

Consider a steady state of confined seepage below a dam discussed in Ref. [33], the elevation of the dam is shown in Fig.9. The dam rests over soil composed of two permeable layers and one impermeable layer, and a cutoff wall is designed in the bottom of the dam for preventing excessive seepage. The water height in the upstream side of the dam is denoted by h_D (m) which is modeled as a random variable following uniform distribution of $U\left(7[m],10[m]\right)$. The hydraulic head h_W over the segment AB with respect to the impermeable layer is equal to $h_W = h_D + 20[m]$. The water flows through two permeable soil layers towards the downstream side of the dam (see segment CD in Fig. 9). It is assumed that there is no water flow on any of the boundaries excepted the segments AB and CD. The first permeable layer is silty sand, while the second one is composed of silty gravel. The permeability of them are modeled as anisotropic and characterized by lognormal random variables, the mean (denoted by m, i.e., $m_{k_{xx,i}}$) and c.o.v. of the horizontal (denoted by $k_{xx,i}$) and vertical permeability (denoted by $k_{yy,i}$) of the two soil layers are provided in Table 6. Note that the c.o.v. associated with each permeability is equal to 100%, indicating a high degree of uncertainty when estimating the parameters in engineering applications. The governing partial differential equation of the seepage problem is

$$k_{xx,i}\frac{\partial^2 h_W}{\partial x^2} + k_{yy,i}\frac{\partial^2 h_W}{\partial y^2} = 0, i = 1,2 \tag{43}$$

The boundary conditions are the hydraulic head over segments AB and CD. A finite element mesh comprising 3413 nodes and 1628 quadratic triangular elements is established for solving the above equation. And the seepage q at the downstream side is measured in volume over time (hour) over distance (meter), i.e., the units of q is $[L/\mathrm{h}/\mathrm{m}]$, it can be calculated by

$$q = -\int_{CD} k_{yy,2}\frac{\partial h_W}{\partial y}\mathrm{d}x \tag{44}$$

The failure event of interest is defined when seepage q exceeds a prescribed threshold $33[L/\mathrm{h}/\mathrm{m}]$. Summarily, the permeability of the permeable layers are modeled as imprecise random variables, while water height h_D is modeled as a precise uniform random variable, and LSF is $g(\boldsymbol{x}) = 33 - q(\boldsymbol{x})$.

First, we set the fixed point $\boldsymbol{\theta}^*$ as $\left(k_{xx,1}^*, k_{yy,1}^*, k_{xx,2}^*, k_{yy,2}^*\right) = (5,2,50,20)$ [10^{-7}m/s] and implementing AFOSM method after transforming into standard normal space, the important direction is $\boldsymbol{e}_\alpha = (0.8094, 0.3949, 0.2826, 0.2491, 0.2168)^T$ corresponding to the five variables in Table 6 by using 152 times of model evaluations. The proposed HA-ILS and WI-ILS are implemented by sampling 100 lines in which the total number of model evaluation are 452. The computational results of first-order component functions are plotted in Fig.10. It is shown that the results of both methods match well with each other and there is a clear trend of linear increase among all the first-order functions. The SDs in Fig.10 vary in the magnitude of 10^{-6} which is two orders of magnitude smaller than the corresponding component functions, revealing that all the first-order estimators are robustly estimated. Since WI-ILS does not involve approximations, so its plot is a relatively more accurate result, and the

small deviation in the third subplot of $P_{fi}\left(m_{k_{xx,2}}\right)$ confirms the bias in HA-ILS method. Additionally, the plots of SDs also show a slower convergence speed away from $\boldsymbol{\theta}^*$, this indicates that the utilized important direction is suboptimal for estimating the actual values of the components as the distance between $\boldsymbol{\theta}$ and $\boldsymbol{\theta}^*$ increases.

The first- and second-order parametric sensitivity indices as well as their SDs and constant component $P_f\left(\theta^*\right)$ are provided in Table 7. Comparing the values of indices one can find that $m_{k_{xx,1}}$ is the most influential parameter among all the indices, and first-order indices are much larger than second-order indices, indicating that the four parameters have a weak interaction effect on failure probability. Fig.11 shows the 3D plot of $P_{fij}\left(m_{k_{xx,1}}, m_{k_{yy,1}}\right)$ and the corresponding SDs for illustrating the trend of second-order components with the proposed two methods. By comparing it with Fig.8 in shallow foundation model, there exist two maximum points in Fig.11 while there is only one in Fig.8. Overall, the plot of first-order and second-order component functions provide a deeper insight into the relationship between failure probability and distribution parameters.

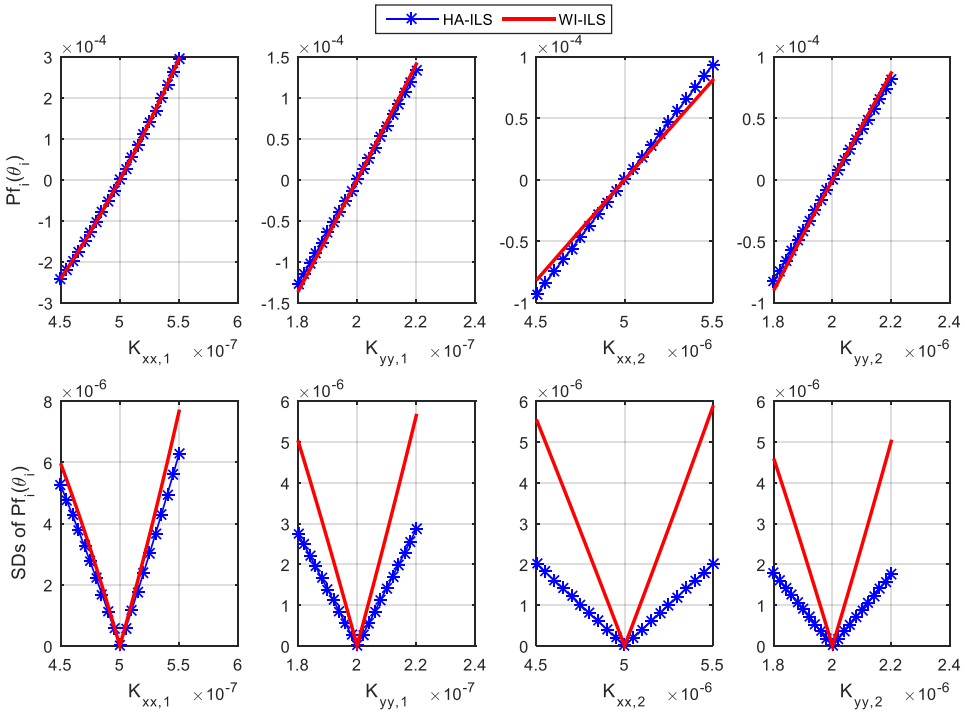

Fig.10 Plots of first-order component functions for confined seepage model

Table 7 The first- and second-order sensitivity indices for confined seepage model

Methods		HA-ILS	WI-ILS
N_{call}		452	452
$P_f\left(\theta^*\right)$		8.088e-4$^{(1.8e-5)}$	8.088e-4$^{(1.8e-5)}$
S_i	$m_{k_{xx,1}}$	0.6796$^{(0.0003)}$	0.6714$^{(0.0004)}$
	$m_{k_{yy,1}}$	0.1618$^{(0.0001)}$	0.1812$^{(0.0002)}$
	$m_{k_{xx,2}}$	0.0831$^{(3e-5)}$	0.0612$^{(0.0003)}$
	$m_{k_{yy,2}}$	0.0646$^{(2e-5)}$	0.0735$^{(0.0002)}$
S_{ij}	$\left(m_{k_{xx,1}}, m_{k_{yy,1}}\right)$	0.0050$^{(2e-6)}$	0.0060$^{(9e-5)}$
	$\left(m_{k_{xx,1}}, m_{k_{xx,2}}\right)$	0.0026$^{(1e-6)}$	0.0018$^{(1e-5)}$
	$\left(m_{k_{xx,1}}, m_{k_{yy,2}}\right)$	0.0020$^{(8e-7)}$	0.0024$^{(8e-6)}$
	$\left(m_{k_{yy,1}}, m_{k_{xx,2}}\right)$	0.0006$^{(2e-7)}$	0.0006$^{(4e-6)}$
	$\left(m_{k_{yy,1}}, m_{k_{yy,2}}\right)$	0.0005$^{(2e-7)}$	0.0007$^{(4e-6)}$
	$\left(m_{k_{xx,2}}, m_{k_{yy,2}}\right)$	0.0002$^{(9e-8)}$	0.0002$^{(3e-6)}$

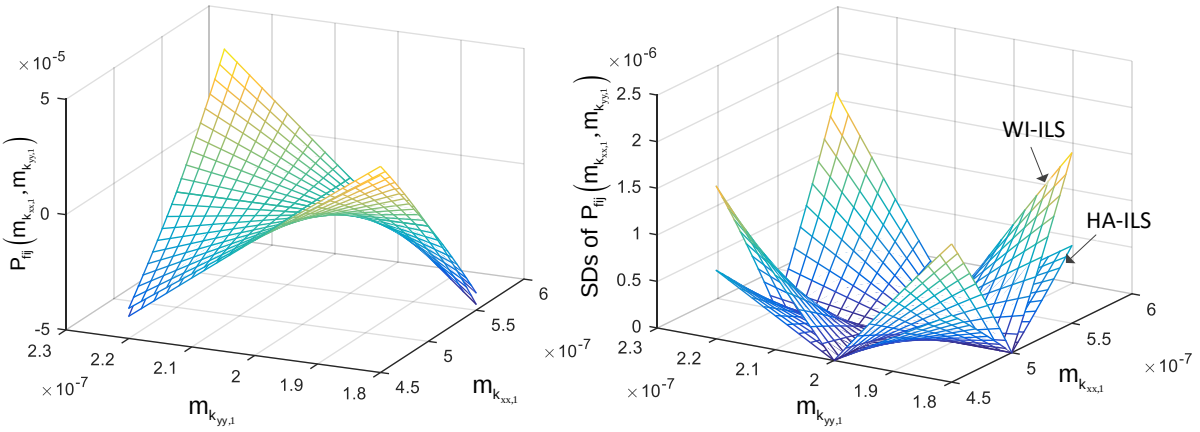

Fig.11 Plots of the two most influential second-order component function with both HA-ILS and WI-ILS method for confined seepage model

4.4 Transmission tower

A model partially based on the example in Ref.[34] is considered, which comprises a considerable number of uncertain parameters. It consists of a truss structure with 80 bars representing a transmission tower (see Fig.12) that behaves within the linear elastic range, and it withstands four static loads in its

top nodes. The four loads are applied in direction $\left[\sin(\pi/3),\cos(\pi/3),0\right]$ and are characterized as deterministic with magnitude F=200 [kN]. Each of the 80 bars contains two random variables, Young's modulus, and the cross-section area, so the total number of random variables is 160. The Young's modulus in each bar is modeled by a lognormal distribution, denoted by $(E_1,\cdots,E_{80})$. The cross-section area is also modeled considering a lognormal distribution, the area for the corner bars is denoted by $\left(A_1^c,\cdots,A_{20}^c\right)$, while the cross-section area for the rest 60 bars is denoted by $\left(A_{21},\cdots,A_{80}\right)$.

The c.o.v. of 10% is considered for all the 160 lognormal random variables, the mean value of both Young's modulus and cross-section area of corner bars are modeled as 40 imprecise parameters (denoted by $m_{E_1},\cdots,m_{E_{20}}$ and $m_{A_1^c},\cdots,m_{A_{20}^c}$), while the mean value of the rest random variables are precisely known. All the parameters of the random variables are listed in Table 8. The response of interest is the displacement of node A located at the top of the transmission tower, which should not exceed a prescribed threshold of 0.06 [m].

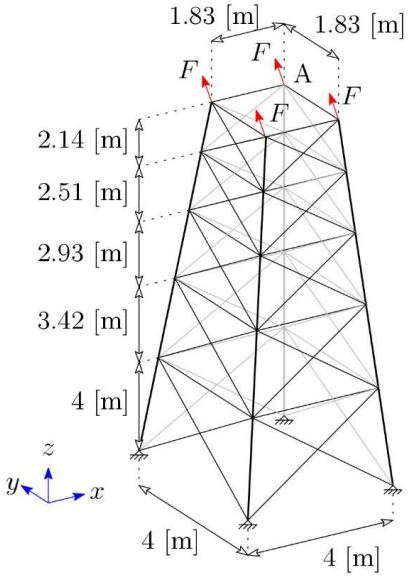

Fig.12 Sketch of transmission tower

Table 8 Distribution parameters of 160 imprecise random variables in transmission tower model

Variable	Description	Distribution	Mean	c.o.v.
$(E_1,\cdots,E_{20})$	Young's modulus of bars 1~20	Lognormal	$[1.89,2.31]\times10^{11}$ [Pa]	10%
$(E_{21},\cdots,E_{80})$	Young's modulus of bars 21~80	Lognormal	2.1×10^{11} [Pa]	10%
$\left(A_1^c,\cdots,A_{20}^c\right)$	Cross-section area of 20 corner bars	Lognormal	[6700,8200] [mm^2]	10%
$\left(A_{21},\cdots,A_{80}\right)$	Cross-section area of the rest 60 bars	Lognormal	4350 [mm^2]	10%

The expansion points θ^* of the 40 imprecise parameters are all set at the middle value of the intervals. Both methods are implemented with the same set 5000 lines with the total number of g-function calls being 15056. Note that line sampling is implemented considering a relatively high

number of lines; such number is selected in order to verify and compare the behavior of the proposed two methods with crude MCS. The constant HDMR component is estimated by both methods as 0.0016 with SD being $8.085e^{-5}$, and the reference result computed by crude MCS is 0.0015 with SD computed to be $7.145e^{-5}$, indicating that the results computed by LS are accurate and robust. With the same set of samples, the first-order sensitivity indices as well as the corresponding plots of component functions are reported in Fig. 13 and Fig. 14, respectively. The sensitivity indices are normalized by the summation of the first two order non-normalized sensitivity indices.

As can be seen from Fig. 13, the first-order sensitivity indices computed by HA-ILS and WI-ILS methods show some differences, which is caused by the failure of computing the indices of the two less important components of E_{17} and A_{17}^c by HA-ILS. The first-order influential components computed by DL are also reported in Fig. 14 for comparison. It is shown that all the first-order influential components are accurately estimated by the WI-ILS method. However, while HA-ILS is utilized, the estimates of the two most influential components of E_{16} and A_{16}^c are accurate, but those of the two less important components of E_{17} and A_{17}^c is not. The reason has been reported in the analytical example, which is due to the inability of identifying these two less influential dimensions in the important direction. However, this can be improved by utilizing some other advanced method for searching another more accurate MPP, instead of the AFOSM method which does not identify all the influential dimensions in this implementation with high accuracy. This indicates that the performance of HA-ILS is highly dependent on the identified important direction, to which WI-ILS is much less sensitive.

The six most important second-order component functions computed by WI-ILS method with the same set of samples are then reported in Fig. 15. The SDs of all estimates are very small and are not reported here. The sensitivity indices of all the influential components reported in Fig. 13 and Fig. 15 sum up to 0.86, indicating that it is accurate to approximate the failure probability function with these components. For higher accuracy, the residual less influential components can be added, and we don't give more details for simplicity.

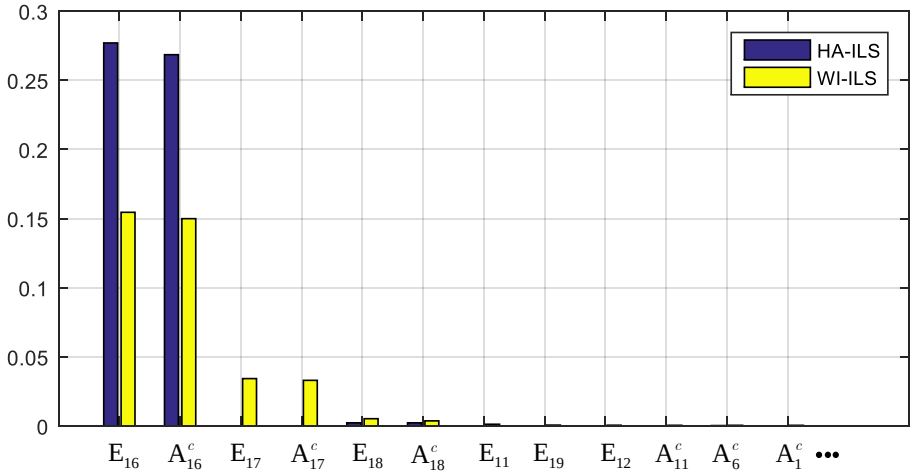

Fig.13 Barplot of the influential first-order sensitivity indices for transmission tower model

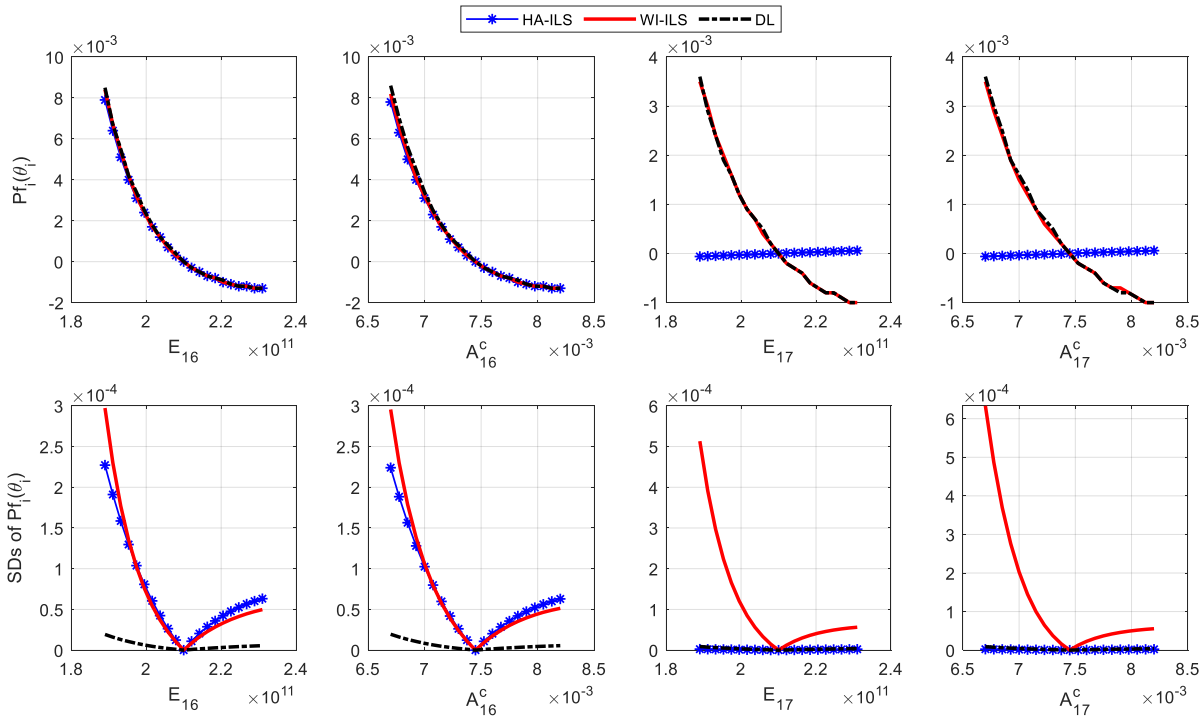

Fig.14 Plots of the four most influential first-order component functions for transmission tower model

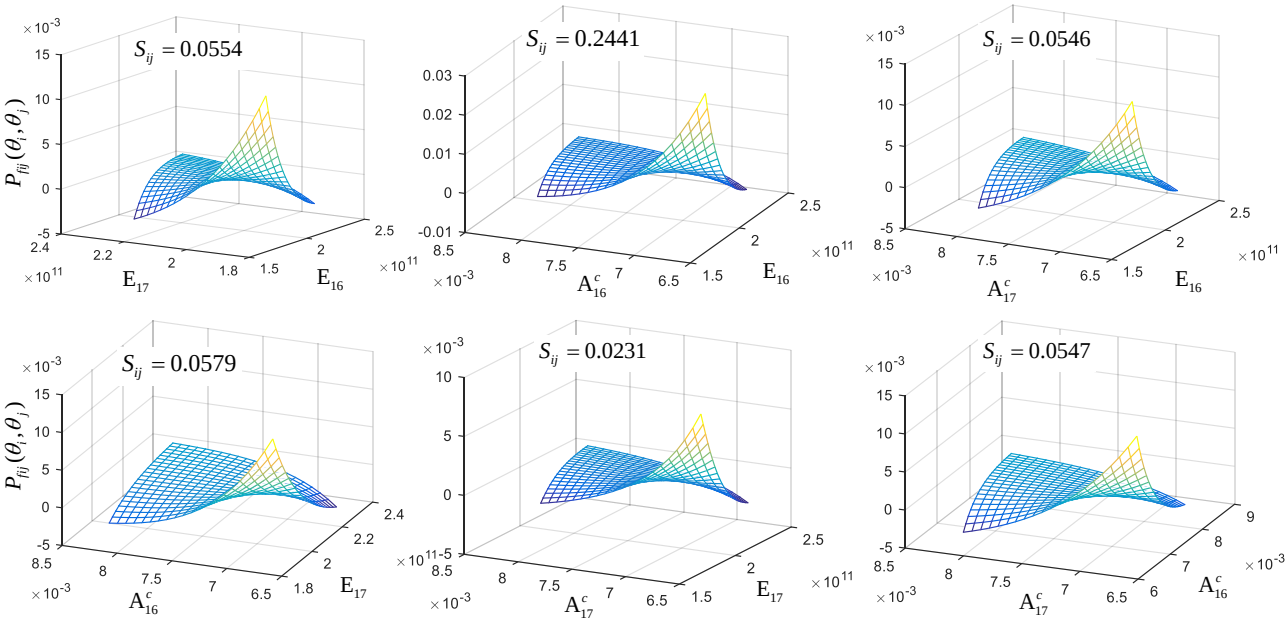

Fig.15 Plots of the six most influential second-order component functions by WI-ILS for transmission tower model

5. Conclusions

The present study was designed to develop efficient simulation methods for reliability analysis subjected to rare failure events when the model input variables are characterized by imprecise probabilities due to the imperfect knowledge. It is realized by developing two strategies for injecting the classical line sampling into the newly developed NISS framework. The first strategy, denoted as HA-ILS, is based on establishing a series of auxiliary hyperplanes for approximating the real LSF with

the input distribution parameters being fixed, and then evaluating the probability mass of the failure domain specified by each hyperplane when the distribution parameters vary. The second strategy, abbreviated as WI-ILS, is developed based on the combination of the simulation in (n-1)-dimensional subspace and the one-dimensional integral along each line. Analytical formulas of failure probability component functions associated with the proposed two methods are discussed in detail when the distribution of model inputs are specified as normal or lognormal independent distributions.

An analytical example and three engineering examples are introduced for demonstrating the two proposed methods, and the main conclusions are as follows. Firstly, the results estimated by HA-ILS and WI-ILS all match well with the reference results by sharing only one small set of samples, indicating that both methods are effective and highly efficient for real applications. Secondly, for weakly or mildly non-linear models with small parameter ranges, HA-ILS has generally a faster convergence speed than WI-ILS, but in the meantime, it may produce a biased result caused by LSF approximations. Thirdly, as $\boldsymbol{\theta}$ is far away from $\boldsymbol{\theta}^*$, the hyperplane approximation of LSF used in HA-ILS might become worse especially for non-linear models. As for WI-ILS, although it doesn't involve approximations, but the utilized important direction will become more and more suboptimal which will undoubtedly lead to a slower convergence speed of the estimators (that is, larger variance). Besides, our method can also evaluate the high-order component functions based on the same set of LS samples, and their relative importance is measured by the sensitivity indices. Thus, in our development, it really doesn't matter whether the higher-order effects are influential or not. The only difference is that, for higher-order component functions, the statistical errors (measured by variances of estimators) can be larger. But for linear or moderately nonlinear problems, the statistical errors increases slowly w.r.t to the orders of components.

Results of the transmission tower show that, for high-dimensional problems with a small number of dimensions being influential, the WI-ILS method is still efficient and accurate for all cut-HDMR components, whereas, the HA-ILS may be ineffective for estimating the less influential components due to the inability of including these dimensions in the important directions. This indicates that, the HA-ILS method is highly dependent on the identified directions, while WI-ILS is not.

Future extensions of the two approaches reported herein, that is HA-ILS and WI-ILS, involve two main aspects. The first one is the analysis of problems involving several failure criteria, which in turn may demand identifying several important directions. Such issue has not been fully addressed in the literature, even when applying Line Sampling to purely aleatoric reliability problems. The second one is addressing the loss of precision (that is, increased variability) of the cut-HDMR estimators when evaluating probabilities for values of the parameter vector $\boldsymbol{\theta}$ that are far away from the reference value $\boldsymbol{\theta}^*$. It is envisioned that such problems could be addressed by performing a more exhaustive exploration of the uncertain parameter space, by switching from a local NISS to its global counterpart.

Acknowledgment

This work is supported by National Natural Science Foundation of China (NSFC) under grant number 51905430. The first author is supported by the program of China Scholarship Council (CSC). The second and third authors are both supported by the Alexander von Humboldt Foundation of Germany. The second author also acknowledges the support by CONICYT (National Commission for Scientific and Technological Research) under grant number 1180271.

Appendix A : Derivation of failure probability function for Eq.(35)

The PDF weight η in Eq.(34) can be further expressed by

$$\eta\left(\boldsymbol{z}^{\perp(s)}+\bar{z}\boldsymbol{e}_{\boldsymbol{\alpha}},\boldsymbol{\theta},\boldsymbol{\theta}^{*}\right)=\left(\prod\nolimits_{d=1}^{n}\frac{\sigma_d^{*}}{\sigma_d}\right)\exp\left(\sum_{d=1}^{n}\left(\frac{\left(z_d^{\perp(s)}+\bar{z}e_{\boldsymbol{\alpha},d}\right)^2}{2}-\frac{\left(\mu_d^{*}+\sigma_d^{*}z_d^{\perp(s)}+\sigma_d^{*}\bar{z}e_{\boldsymbol{\alpha},d}-\mu_d\right)^2}{2\sigma_d^2}\right)\right) \quad \text{(A.1)}$$

Let ξ denote the first term above

$$\xi=\left(\prod\nolimits_{d=1}^{n}\frac{\sigma_d^{*}}{\sigma_d}\right) \quad \text{(A.2)}$$

As for the second term, it can be derived further as

$$\exp\left(\sum\nolimits_{d=1}^{n}\left(\frac{\left(z_d^{\perp(s)}\right)^2}{2}-\frac{\left(\mu_d^{*}+\sigma_d^{*}z_d^{\perp(s)}-\mu_d\right)^2}{2\sigma_d^2}\right)+\bar{z}\sum\nolimits_{d=1}^{n}\left(z_d^{\perp(s)}e_{\boldsymbol{\alpha},d}-\frac{\left(\mu_d^{*}+\sigma_d^{*}z_d^{\perp(s)}-\mu_d\right)\sigma_d^{*}e_{\boldsymbol{\alpha},d}}{\sigma_d^2}\right)+\bar{z}^2\sum\nolimits_{d=1}^{n}\left(\frac{e_{\boldsymbol{\alpha},d}^2}{2}\left(1-\frac{\sigma_d^{*2}}{\sigma_d^2}\right)\right)\right) \quad \text{(A.3)}$$

Let $\lambda^{(s)}$, $\kappa^{(s)}$, ζ denote the above three terms, respectively, i.e.,

$$\begin{aligned}
\lambda^{(s)}&=\sum\nolimits_{d=1}^{n}\left(\frac{\left(z_d^{\perp(s)}\right)^2}{2}-\frac{\left(\mu_d^{*}+\sigma_d^{*}z_d^{\perp(s)}-\mu_d\right)^2}{2\sigma_d^2}\right)\\
\kappa^{(s)}&=\sum\nolimits_{d=1}^{n}\left(z_d^{\perp(s)}e_{\boldsymbol{\alpha},d}-\frac{\left(\mu_d^{*}+\sigma_d^{*}z_d^{\perp(s)}-\mu_d\right)\sigma_d^{*}e_{\boldsymbol{\alpha},d}}{\sigma_d^2}\right)\\
\zeta&=\sum\nolimits_{d=1}^{n}\left(\frac{e_{\boldsymbol{\alpha},d}^2}{2}\left(1-\frac{\sigma_d^{*2}}{\sigma_d^2}\right)\right)
\end{aligned} \quad \text{(A.4)}$$

Note that ξ, ζ, $\lambda^{(s)}$, $\kappa^{(s)}$ are all functions of distribution parameters $\boldsymbol{\mu}$ and $\boldsymbol{\sigma}$, and $\zeta\le 1/2$. Additionally, $\lambda^{(s)}$, $\kappa^{(s)}$ vary according to the value of sample $z_d^{\perp(s)}$. Then the PDF weight is simplified as

$$\eta\left(\boldsymbol{z}^{\perp(s)}+\bar{z}\boldsymbol{e}_{\boldsymbol{\alpha}},\boldsymbol{\theta},\boldsymbol{\theta}^{*}\right)=\xi\exp\left(\lambda^{(s)}+\bar{z}\kappa^{(s)}+\bar{z}^2\zeta\right) \quad \text{(A.5)}$$

Taking it into Eq.(31) one derives

$$L^{(s)}\left(\boldsymbol{\mu},\boldsymbol{\sigma}\right)=\xi e^{\lambda^{(s)}}\int_{\tilde{c}^{(s)}}^{\infty}\exp\left(\bar{z}\kappa^{(s)}+\bar{z}^2\zeta\right)\phi\left(\bar{z}\right)\mathrm{d}\bar{z} \quad \text{(A.6)}$$

The integral $\int_{\tilde{c}^{(s)}}^{\infty}\exp\left(\bar{z}\kappa^{(s)}+\bar{z}^2\zeta\right)\phi\left(\bar{z}\right)\mathrm{d}\bar{z}$ can furtherly derived with an analytical solution

$$\int_{\tilde{c}^{(s)}}^{\infty}\exp\left(\bar{z}\kappa^{(s)}+\bar{z}^2\zeta\right)\phi\left(\bar{z}\right)\mathrm{d}\bar{z}=\int_{\tilde{c}^{(s)}}^{\infty}\frac{1}{\sqrt{2\pi}}\exp\left(\left(\zeta-\frac{1}{2}\right)\bar{z}^2+\kappa^{(s)}\bar{z}\right)\mathrm{d}\bar{z}$$

$$=\int_{\tilde{c}^{(s)}}^{\infty}\frac{1}{\sqrt{2\pi}}\exp\left(-\frac{1}{2}\left(\left(1-2\zeta\right)\bar{z}^2-2\kappa^{(s)}\bar{z}+\frac{\left(\kappa^{(s)}\right)^2}{1-2\zeta}\right)+\frac{\left(\kappa^{(s)}\right)^2}{2-4\zeta}\right)\mathrm{d}\bar{z}$$

$$=\exp\left(\frac{\left(\kappa^{(s)}\right)^2}{2-4\zeta}\right)\int_{\tilde{c}^{(s)}}^{\infty}\frac{1}{\sqrt{2\pi}}\exp\left(-\frac{1}{2}\left(\sqrt{1-2\zeta}\,\bar{z}-\frac{\kappa^{(s)}}{\sqrt{1-2\zeta}}\right)^2\right)\mathrm{d}\bar{z} \tag{A.7}$$

Let $\sqrt{1-2\zeta}\,\bar{z}-\frac{\kappa^{(s)}}{\sqrt{1-2\zeta}}=t$, where $t\in[\sqrt{1-2\zeta}\tilde{c}^{(s)}-\frac{\kappa^{(s)}}{\sqrt{1-2\zeta}},+\infty)$, the above integral can be derived as

$$\int_{\tilde{c}^{(s)}}^{\infty}\exp\left(\bar{z}\kappa^{(s)}+\bar{z}^2\zeta\right)\phi\left(\bar{z}\right)\mathrm{d}\bar{z}=\exp\left(\frac{\left(\kappa^{(s)}\right)^2}{2-4\zeta}\right)\int_{\sqrt{1-2\zeta}\tilde{c}^{(s)}-\frac{\kappa^{(s)}}{\sqrt{1-2\zeta}}}^{\infty}\frac{1}{\sqrt{2\pi}}\mathrm{e}^{-\frac{1}{2}t^2}\,\mathrm{d}\left(\frac{1}{\sqrt{1-2\zeta}}t+\frac{\kappa^{(s)}}{1-2\zeta}\right)$$

$$=\frac{1}{\sqrt{1-2\zeta}}\exp\left(\frac{\left(\kappa^{(s)}\right)^2}{2-4\zeta}\right)\Phi\left(-\left(\sqrt{1-2\zeta}\tilde{c}^{(s)}-\frac{\kappa^{(s)}}{\sqrt{1-2\zeta}}\right)\right) \tag{A.8}$$

$$=\frac{1}{\sqrt{1-2\zeta}}\exp\left(\frac{\left(\kappa^{(s)}\right)^2}{2-4\zeta}\right)\Phi\left(\frac{\kappa^{(s)}-\left(1-2\zeta\right)c^{(s)}}{\sqrt{1-2\zeta}}\right)$$

Then the analytical expression of the integral is finally derived as

$$L^{(s)}\left(\boldsymbol{\mu},\boldsymbol{\sigma}\right)=\frac{\xi}{\sqrt{1-2\zeta}}\exp\left(\lambda^{(s)}+\frac{\left(\kappa^{(s)}\right)^2}{2-4\zeta}\right)\Phi\left(\frac{\kappa^{(s)}-\left(1-2\zeta\right)c^{(s)}}{\sqrt{1-2\zeta}}\right) \tag{A.9}$$

Appendix B：Derivation of analytical failure probability function of Eq.(41)

In standard normal space, the performance function in Eq.(40) is expressed as $h\left(z_1,z_2\right)=\beta-\left(\mu_1+\sigma_1 z_1\right)+\kappa\left(\mu_2+\sigma_2 z_2\right)^2$. The boundary of LSF $h\left(z_1,z_2\right)=0$ can be drawn as shown in Fig.B1. Assume that z_2' is a realization of z_2, then search the value of z_1' that satisfies the equation $h\left(z_1,z_2'\right)=0$, i.e.,

$$z_1'=\frac{\beta-\mu_1}{\sigma_1}+\frac{\kappa}{\sigma_1}\left(\mu_2+\sigma_2 z_2'\right)^2 \tag{B.1}$$

From the view of line sampling, the reliability index associated with z_2' is actually the distance d_1 shown in Fig.B1, and its value equals to z_1'. As a consequence, the failure probability can be expressed analytically with the following one-dimensional integral,

$$P_f\left(\mu_1,\mu_2,\sigma_1,\sigma_2\right)=\int_{-\infty}^{+\infty}\Phi\left(-z_1'\right)\phi\left(z_2\right)\mathrm{d}z_2$$

$$=\int_{-\infty}^{+\infty}\Phi\left(-\frac{\beta-\mu_1}{\sigma_1}-\frac{\kappa}{\sigma_1}\left(\mu_2+\sigma_2 z_2\right)^2\right)\phi\left(z_2\right)\mathrm{d}z_2 \tag{B.2}$$

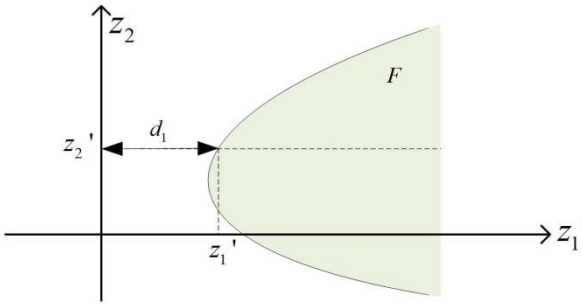

Fig.B1 Geometric sketch for deriving analytical solution of failure probability

References

[1]. Faes M, Broggi M, Patelli E, et al. A multivariate interval approach for inverse uncertainty quantification with limited experimental data. Mechanical Systems and Signal Processing, 2019, 118: 534-548.

[2]. Hohenbichler M, Gollwitzer S, Kruse W, et al. New light on first-and second-order reliability methods. Structural Safety, 1987, 4(4): 267-284.

[3]. Ghanem R G, Spanos P D. Stochastic finite elements: a spectral approach. Courier Corporation, 2003.

[4]. Au S K, Beck J L. Estimation of small failure probabilities in high dimensions by subset simulation. Probabilistic Engineering Mechanics, 2001, 16(4): 263-277.

[5]. Li J, Chen J. The principle of preservation of probability and the generalized density evolution equation. Structural Safety, 2008, 30(1): 65-77.

[6]. Faes M, Moens D. Recent Trends in the Modeling and Quantification of Non-probabilistic Uncertainty. Archives of Computational Methods in Engineering, 2019: 1-39.

[7]. Der Kiureghian A, Ditlevsen O. Aleatory or epistemic? Does it matter?. Structural Safety, 2009, 31(2): 105-112.

[8]. Beer M, Ferson S, Kreinovich V. Imprecise probabilities in engineering analyses. Mechanical systems and signal processing, 2013, 37(1-2): 4-29.

[9]. Zhang H, Mullen R L, Muhanna R L. Interval Monte Carlo methods for structural reliability. Structural Safety, 2010, 32(3): 183-190.

[10]. Alvarez D A, Uribe F, Hurtado J E. Estimation of the lower and upper bounds on the probability of failure using subset simulation and random set theory. Mechanical Systems and Signal Processing, 2018, 100: 782-801.

[11]. Zhang Z, Jiang C, Wang G G, et al. First and second order approximate reliability analysis methods using evidence theory. Reliability Engineering & System Safety, 2015, 137: 40-49.

[12]. Wei P, Song J, Bi S, et al. Non-intrusive stochastic analysis with parameterized imprecise probability models: I. Performance estimation. Mechanical Systems and Signal Processing, 2019, 124: 349-368.

[13]. Wei P, Song J, Bi S, et al. Non-intrusive stochastic analysis with parameterized imprecise probability models: II. Reliability and rare events analysis. Mechanical Systems and Signal Processing, 2019, 126: 227-247.

[14]. Wei P, Lu Z, Song J. Extended Monte Carlo simulation for parametric global sensitivity analysis and optimization. AIAA Journal, 2014, 52(4): 867-878.

[15]. Li G, Wang S W, Rosenthal C, et al. High dimensional model representations generated from low dimensional data samples. I. mp-Cut-HDMR. Journal of Mathematical Chemistry, 2001, 30(1): 1-30.

[16]. Li G, Rabitz H. General formulation of HDMR component functions with independent and correlated variables. Journal of Mathematical Chemistry, 2012, 50(1): 99-130.

[17]. Kaya H, Kaplan M, Saygın H. A recursive algorithm for finding HDMR terms for sensitivity analysis. Computer Physics Communications, 2004, 158(2):106-12.

[18]. Schuëller G I, Pradlwarter H J, Koutsourelakis P S. A critical appraisal of reliability estimation procedures for high dimensions. Probabilistic engineering mechanics, 2004, 19(4): 463-474.

[19]. Koutsourelakis P S, Pradlwarter H J, Schuëller G I. Reliability of structures in high dimensions, part I: algorithms and applications. Probabilistic Engineering Mechanics, 2004, 19(4): 409-417.

[20]. Hohenbichler M, Rackwitz R. Improvement of second-order reliability estimates by importance sampling. Journal of Engineering Mechanics, 1988, 114(12): 2195-2199.

[21]. Rackwitz R. Reliability analysis—a review and some perspectives. Structural safety, 2001, 23(4): 365-395.

[22]. Song J, Lu Z, Wei P, et al. Global sensitivity analysis for model with random inputs characterized by probability-box. Proceedings of the Institution of Mechanical Engineers, Part O: Journal of Risk and Reliability, 2015, 229(3): 237-253.

[23]. Chen L, Wang H, Ye F, et al. Comparative study of HDMRs and other popular metamodeling techniques for high dimensional problems. Structural and Multidisciplinary Optimization, 2019, 59(1): 21-42.

[24]. Wei P, Lu Z, Song J. Variable importance analysis: a comprehensive review. Reliability Engineering & System Safety, 2015, 142: 399-432.

[25]. Schuëller G I. Efficient Monte Carlo simulation procedures in structural uncertainty and reliability analysis-recent advances. Structural Engineering and Mechanics, 2009, 32(1): 1-20.

[26]. Lu Z, Song S, Li H, Yuan X. The reliability and reliability sensitivity analysis for structural and mechanical system. Beijing, China: Science Press, 2009, pp. 179-181.

[27]. Pradlwarter H J, Schuëller G I, Koutsourelakis P S, et al. Application of line sampling simulation method to reliability benchmark problems. Structural Safety, 2007, 29(3): 208-221.

[28]. Pradlwarter H J, Pellissetti M F, Schenk C A, et al. Realistic and efficient reliability estimation for aerospace structures. Computer Methods in Applied Mechanics and Engineering, 2005, 194(12-16): 1597-1617.

[29]. Lu Z, Song S, Yue Z, et al. Reliability sensitivity method by line sampling. Structural Safety, 2008, 30(6): 517-532.

[30]. De Angelis M, Patelli E, Beer M. Advanced line sampling for efficient robust reliability analysis. Structural Safety, 2015, 52: 170-182.

[31]. Depina I, Le T M H, Fenton G, et al. Reliability analysis with metamodel line sampling. Structural Safety, 2016, 60: 1-15.

[32]. Valdebenito M A, Jensen H A, Beer M, et al. Approximation Concepts For Fuzzy Structural Analysis , Proceedings of the Second International Conference on Vulnerability and Risk Analysis and Management (ICVRAM), ASCE Council on Disaster Risk Management, Monograph No 9, CD-ROM, 2014, 135-144.

[33]. Valdebenito M A, Jensen H A, Hernández H B, et al. Sensitivity estimation of failure probability applying line sampling. Reliability Engineering & System Safety, 2018, 171: 99-111.

[34]. Haukaas T, Der Kiureghian A. Strategies for finding the design point in non-linear finite element reliability analysis. Probabilistic Engineering Mechanics, 2006, 21(2), 133-147.